



HELLENIC REPUBLIC

**National and Kapodistrian
University of Athens**

— EST. 1837 —

Department of Economics

M.Sc. in Business Administration, Analytics and Information Systems

**Numerical Evidence of the Lagrange Multipliers in Piecewise
Monotonic Data Approximation Method**

Ioannis N. Perdikas

**Supervisor Professor
Ioannis C. Demetriou**

Athens

March 2019



HELLENIC REPUBLIC

**National and Kapodistrian
University of Athens**

— EST. 1837 —

Department of Economics

M.Sc. in Business Administration, Analytics and Information Systems

**Numerical Evidence of the Lagrange Multipliers in Piecewise
Monotonic Data Approximation Method**

Ioannis N. Perdikas

**Supervisor Professor
Ioannis C. Demetriou**

Athens

March 2019

Copyright © Πέρδικας Ιωάννης, 2019

Με επιφύλαξη παντός δικαιώματος. All rights reserved.

Η έγκριση της διπλωματικής εργασίας από το Τμήμα Οικονομικών Επιστημών (ΠΜΣ Διοίκηση, Αναλυτική και Πληροφοριακά Συστήματα Επιχειρήσεων) του Εθνικού και Καποδιστριακού Πανεπιστημίου Αθηνών δεν υποδηλώνει απαραίτητως και αποδοχή των απόψεων του συγγραφέα εκ μέρους του Τμήματος.

«Ο υποψήφιος βεβαιώνει ότι η υποβληθείσα εργασία είναι προσωπική εκτός από τα σημεία όπου γίνεται αναφορά στις εργασίες άλλων»

Ιωάννης Ν. Πέρδικας

Acknowledgements

This thesis becomes a reality with the kind support and help of many individuals. I would like to extend my sincere thanks to all of them.

I would like to express my special gratitude and thanks to my advisor, Professor Ioannis C. Demetriou for imparting his knowledge and expertise in this study.

My thanks and appreciations also go to my colleague and people who have willingly helped me out with their abilities.

Contents

Figures	7
Tables	9
Abstract	11
1 Introduction	13
1.1 The problem of data approximation	13
1.1.1 Least squares data fitting	13
1.1.2 Piecewise monotonic approximation	16
1.2 Non-linear programming problem and Lagrange multipliers	17
1.2.1 Non-linear programming problem	17
1.2.2 First order conditions for equality constraints	18
1.2.3 Quadratic objective function and linear equality constraints	20
1.2.4 First order conditions for inequality constraints	22
2 Piecewise monotonic data approximation	25
2.1 Definition of piecewise monotonic data approximation	25
2.2 The monotonic problem	27
2.3 Lagrange multipliers in the monotonic case	29
3 Experimental Results	31
3.1 Setting the experiment	31
3.2 The Raman spectrum of zircon	33
3.3 Experiments with Raman spectra of minerals	40
3.3.1 The Raman spectrum of datolite	40
3.3.2 The Raman spectrum of olivenite	42
3.3.3 The Raman spectrum of clintonite	44
3.3.4 The Raman spectrum of beryl	46

3.3.5	The Raman spectrum of lizardite	48
3.3.6	The Raman spectrum of hemimorphite	50
3.3.7	The Raman spectrum of wulfenite	52
3.4	Experiments on turning point separation	54
3.4.1	The MS spectrum of diiodothyronine	55
3.4.2	The Raman spectrum of cellulose	57
4	Discussion and Conclusions	60

Figures

2.1	Graphical representation of the data given in Table 2.1. Best monotonic fit with $k = 1$ to 40 data points (plus signs) of $\sin(\pi x) + \varepsilon_i$. The solid line illustrates the best fit.	28
3.1	Detected peaks (circles) by a best monotonic fit with $k = 1$ to 1024 data points (plus signs) of the zircon Raman spectrum. The solid line illustrates the best fit. The numbers give the intensities at the corresponding Raman shifts. . . .	33
3.2	As in Fig. 3.1, but detected peaks by a best monotonic fit with $k = 2$. The peak is indicated by circle.	34
3.3	As in Fig. 3.1, but detected peaks by a best monotonic fit with $k = 3$. The peak is indicated by circle.	34
3.4	As in Fig. 3.1, but detected peaks by a best monotonic fit with $k = 4$. The peaks are indicated by circle.	35
3.5	As in Fig. 3.1, but detected peaks by a best monotonic fit with $k = 6$. The peaks are indicated by circle.	35
3.6	As in Fig. 3.1, but detected peaks by a best monotonic fit with $k = 8$. The peaks are indicated by circle.	36
3.7	As in Fig. 3.1, but detected peaks by a best monotonic fit with $k = 10$. The peaks are indicated by circle.	36
3.8	As in Fig. 3.1, but detected peaks by a best monotonic fit with $k = 12$. The peaks are indicated by circle.	37
3.9	As in Fig. 3.1, but detected peaks by a best monotonic fit with $k = 14$. The peaks are indicated by circle.	37
3.10	As in Fig. 3.1, but detected peaks by a best monotonic fit with $k = 16$. The peaks are indicated by circle.	38

3.11	Detected peaks (circles) by a best monotonic fit with $k = 14$ to 1024 data points (plus signs) of the datolite Raman spectrum. The solid line illustrates the best fit. The numbers give the intensities at the corresponding Raman shifts. . . .	40
3.12	Detected peaks (circles) by a best monotonic fit with $k = 14$ to 1024 data points (plus signs) of the olivenite Raman spectrum. The solid line illustrates the best fit. The numbers give the intensities at the corresponding Raman shifts. . . .	43
3.13	Detected peaks (circles) by a best monotonic fit with $k = 12$ to 1024 data points (plus signs) of the clintonite Raman spectrum. The solid line illustrates the best fit. The numbers give the intensities at the corresponding Raman shifts.	45
3.14	Detected peaks (circles) by a best monotonic fit with $k = 14$ to 1000 data points (plus signs) of the beryl Raman spectrum. The solid line illustrates the best fit. The numbers give the intensities at the corresponding Raman shifts.	47
3.15	Detected peaks (circles) by a best monotonic fit with $k = 14$ to 1008 data points (plus signs) of the lizardite Raman spectrum. The solid line illustrates the best fit. The numbers give the intensities at the corresponding Raman shifts. . .	49
3.16	Detected peaks (circles) by a best monotonic fit with $k = 16$ to 1024 data points (plus signs) of the hemimorphite Raman spectrum. The solid line illustrates the best fit. The numbers give the intensities at the corresponding Raman shifts.	51
3.17	Detected peaks (circles) by a best monotonic fit with $k = 8$ to 1024 data points (plus signs) of the wulfenite Raman spectrum. The solid line illustrates the best fit. The numbers give the intensities at the corresponding Raman shifts.	53
3.18	Detected peaks (circles) by a best monotonic fit with $k = 16$ to 2167 data points (plus signs) of the diiodothyronine Raman spectrum. The solid line illustrates the best fit. The numbers give the intensities at the corresponding Raman shifts.	55
3.19	Detected peaks (circles) by a best monotonic fit with $k = 16$ to 3590 data points (plus signs) of the cellulose Raman spectrum. The solid line illustrates the best fit. The numbers give the intensities at the corresponding Raman shifts. . .	58

Tables

2.1	Best fits with $k = 1$ monotonic sections to measurements of $\sin(\pi x) + \varepsilon_i$	28
3.1	Left four columns: Turning points in the zircon spectrum by a best fit with $k = 16$ monotonic sections. Right eight columns: The turning point positions of the optimal fit for k in $\{2, 4, \dots, 16\}$ are indicated by the times sign	38
3.2	Measures for Zircon.	39
3.3	Left four columns: Turning points in the datolite spectrum by a best fit with $k = 20$ monotonic sections. Right ten columns: The turning point positions of the optimal fit for k in $\{2, 4, \dots, 20\}$ are indicated by the times sign	41
3.4	Measures for Datolite	42
3.5	Left four columns: Turning points in the olivenite spectrum by a best fit with $k = 16$ monotonic sections. Right eight columns: The turning point positions of the optimal fit for k in $\{2, 4, \dots, 16\}$ are indicated by the times sign	43
3.6	Measures for Olivenite	44
3.7	Left four columns: Turning points in the clintonite spectrum by a best fit with $k = 14$ monotonic sections. Right seven columns: The turning point positions of the optimal fit for k in $\{2, 4, \dots, 14\}$ are indicated by the times sign	45
3.8	Measures for Clintonite	46
3.9	Left four columns: Turning points in the beryl spectrum by a best fit with $k = 14$ monotonic sections. Right seven columns: The turning point positions of the optimal fit for k in $\{2, 4, \dots, 14\}$ are indicated by the times sign	47
3.10	Measures for Beryl	48
3.11	Left four columns: Turning points in the lizardite spectrum by a best fit with $k = 14$ monotonic sections. Right seven columns: The turning point positions of the optimal fit for k in $\{2, 4, \dots, 14\}$ are indicated by the times sign	49
3.12	Measures for Lizardite	50

3.13	Left four columns: Turning points in the hemimorphite spectrum by a best fit with $k = 18$ monotonic sections. Right nine columns: The turning point positions of the optimal fit for k in $\{2, 4, \dots, 18\}$ are indicated by the times sign	51
3.14	Measures for Hemimorphite	52
3.15	Left four columns: Turning points in the wulfenite spectrum by a best fit with $k = 16$ monotonic sections. Right eight columns: The turning point positions of the optimal fit for k in $\{2, 4, \dots, 16\}$ are indicated by the times sign	53
3.16	Measures for Wulfenite	54
3.17	Left four columns: Turning points in the diiodothyronine spectrum by a best fit with $k = 16$ monotonic sections. Right eight columns: The turning point positions of the optimal fit for k in $\{2, 4, \dots, 16\}$ are indicated by the times sign^a	56
3.18	Measures for Diiodothyronine	57
3.19	Left four columns: Turning points in the cellulose spectrum by a best fit with $k = 18$ monotonic sections. Right nine columns: The turning point positions of the optimal fit for k in $\{2, 4, \dots, 18\}$ are indicated by the times sign	58
3.20	Measures for Cellulose	59

Abstract

ENGLISH

This thesis investigates the behavior of the Lagrange multipliers at the piecewise monotonic approximation to spectra of minerals, carbohydrate and thyroid hormone. The spectra datasets of minerals are provided freely from Laboratory of Photoinduced Effects Vibrational and X-RAY Spectroscopies [25], of thyroid hormone from Human Metabolome Database [26] and of carbohydrate from SPECARB database [27]. The thesis consists of four chapters.

In chapter 1 we present the problem of data approximation and especially the case of least squares data fitting, how the smoothed data are calculated and expound the piecewise monotonic data approximation. Furthermore, we discuss the non-linear programming problem and Lagrange multipliers in both cases when the constraints are linear equality and linear inequality. In chapter 2 we present the piecewise monotonic data approximation method, we give an example and we state how the Lagrange multipliers are calculated. In chapter 3 we perform experiments using nine Raman spectra, eight of minerals and one of carbohydrate, and one MS spectrum of thyroid hormone in order to determine how Lagrange multipliers are changed as the number of monotonic sections in a piecewise monotonic data approximation is changed. We define the measures which are needed to determine this relationship, we fit each data by the L2WPMA software package for various values of monotonic sections and we present the results. In chapter 4 we present the conclusions from the experiments which lead to develop a Lagrange multiplier test that will provide an estimation of a suitable or adequate number of monotonic sections of the fit.

Keywords: Data smoothing, Least squares method, Lagrange multipliers, Piecewise monotonic data approximation, L2WPMA algorithm

GREEK

‘Αριθμητικά τεκμήρια των πολλαπλασιαστών Lagrange στην κατά τμήματα μονότονη προσέγγιση δεδομένων’

Αυτή η διπλωματική εργασία ερευνά τη συμπεριφορά των πολλαπλασιαστών Lagrange στην κατά τμήματα μονότονη προσέγγιση σε φάσματα ορυκτών, υδατάνθρακα και θυροειδούς ορμόνης. Τα σύνολα δεδομένων των φασμάτων των ορυκτών παρέχονται ελεύθερα από το Laboratory of Photoinduced Effects Vibrational and X-RAY Spectroscopies [25], της θυροειδούς ορμόνης από την βάση δεδομένων Human Metabolome [26] και του υδατάνθρακα από την βάση δεδομένων SPECARB [27]. Η διπλωματική εργασία αποτελείται από τέσσερα κεφάλαια.

Στο κεφάλαιο 1 παρουσιάζουμε το πρόβλημα της προσέγγισης των δεδομένων και ειδικότερα την περίπτωση της προσέγγισης ελαχίστων τετραγώνων, τον τρόπο υπολογισμού των εξομαλυνθέντων δεδομένων και κάνουμε μία πρώτη αναφορά στην κατά τμήματα μονότονη προσέγγιση δεδομένων. Επιπλέον, συζητάμε το πρόβλημα του μη γραμμικού προγραμματισμού και των πολλαπλασιαστών Lagrange στις περιπτώσεις όπου οι γραμμικοί περιορισμοί είναι ισότητες ή ανισότητες. Στο κεφάλαιο 2 παρουσιάζουμε την κατά τμήματα μονότονη προσέγγιση δεδομένων μαζί με ένα παράδειγμα και αναφέρουμε τον τρόπο υπολογισμού των πολλαπλασιαστών Lagrange. Στο κεφάλαιο 3 πραγματοποιούμε πειράματα χρησιμοποιώντας εννέα φάσματα Raman, οκτώ ορυκτών και ενός υδατάνθρακα, και ένα φάσμα MS θυροειδούς ορμόνης, προκειμένου να καθοριστεί ο τρόπος με τον οποίο μεταβάλλονται οι πολλαπλασιαστές Lagrange καθώς ο αριθμός των μονότονων τμημάτων σε μια κατά τμήματα μονότονη προσέγγιση δεδομένων μεταβάλλεται. Ορίζουμε τα μέτρα που χρειάζονται για να καθορίσουμε αυτή την σχέση, τρέχουμε τα δεδομένα στο πακέτο λογισμικού L2WPMA για διάφορες τιμές μονότονων τμημάτων και παρουσιάζουμε τα αποτελέσματα. Στο κεφάλαιο 4 παρουσιάζουμε τα συμπεράσματα από τα πειράματα τα οποία οδηγούν στην ανάπτυξη ενός τεστ πολλαπλασιαστών Lagrange που θα παρέχει μία εκτίμηση ενός κατάλληλου ή επαρκούς αριθμού μονότονων τμημάτων της προσέγγισης.

Λέξεις-κλειδιά: Λείανση δεδομένων, Μέθοδος ελαχίστων τετραγώνων, Κατά τμήματα μονότονη προσέγγιση δεδομένων, Πολλαπλασιαστές Lagrange, L2WPMA αλγόριθμος

Chapter 1

Introduction

1.1 The problem of data approximation

A smooth function $f(x)$, $a \leq x \leq b$ is measured at the points $a = x_1 < x_2 < \dots < x_n = b$ and the measurements $\{\phi_i \approx f(x_i) : i = 1, 2, \dots, n\}$ contain random errors. The general problem of data smoothing or data approximation is to calculate numbers $\{y_i : i = 1, 2, \dots, n\}$ from the measurements that are smooth and that should be closer than the measurements to the true function values $\{f(x_i) : i = 1, 2, \dots, n\}$.

There are many approaches to this problem and in section 1.1.2. we present one that has been used for many years dating to Lagrange. By “close” we mean that one makes least changes to the data subject to some condition that is defined by the user, and there are several ways of defining “least”. A useful choice is to minimize the expression

$$\|\underline{y} - \underline{\phi}\|_2^2 = \sum_{i=1}^n (y_i - \phi_i)^2, \quad (1.1)$$

where $\underline{\phi}$ denotes the vector in \mathbb{R}^n whose components are $\phi_1, \phi_2, \dots, \phi_n$. Expression (1.1) is appropriate when the data errors have a normal distribution (see, Gauss [1]). The “condition” is related to the smoothing approach that is followed by the user.

1.1.1 Least squares data fitting

The material of this section has been based on Hildebrand [6] and Forsythe, Malcolm & Moler [7]. Let $\{(x_i, y_i) : i = 0, 1, \dots, n\}$ be a set of data points. Consider x_i the independent

variable and y_i the dependent variable which satisfy the functional relationship

$$y_i = f(x_i). \quad (1.2)$$

The function f is an unknown function, which is known to exist, but its type is not known. The main purpose is to determine a polynomial of high degree that achieves a best approximation. This ensures that the error of the approach should be as minimal as possible.

Furthermore, in the discrete set of points x_0, x_1, \dots, x_n we suppose that f is to be approximated by y . Its form is the following

$$f(\underline{x}) \approx \sum_{k=0}^m \alpha_k \phi_k(\underline{x}) \equiv y(\underline{x}), \quad \underline{x} \in \mathbb{R}^n, \quad (1.3)$$

where y is linear combination of m coordinate functions $\phi_0, \phi_1, \dots, \phi_m$, although the coordinate functions may be nonlinear functions of x . In the case of the number of the unknown coefficients m is lower than the number of data points n , such that $m + 1 < n$, the problem of choosing the coefficients is overdetermined and it is hardly possible to achieve the best data fitting.

If we determine the residual $R(\underline{x})$ as follows

$$R(\underline{x}) = \sum_{k=0}^m \alpha_k \phi_k(\underline{x}) - f(\underline{x}) \equiv y(\underline{x}) - f(\underline{x}), \quad (1.4)$$

the coefficients α_k , which are chosen to minimize the sum of squares of the residuals, are specified by the least squares criterion, that is,

$$\min \sum_{i=0}^n [R(x_i)]^2 = \min \sum_{i=0}^n \left[\sum_{k=0}^m \alpha_k \phi_k(x_i) - f(x_i) \right]. \quad (1.5)$$

In the special case of the model exactly fitting the data, the previous quantity will be zero, hence interpolation is included.

A unique set of coefficients is defined by the least squares criterion. On condition that the coordinate functions are linearly dependent at the data points, there are nonzero coefficients c_k , such that

$$\sum_{k=0}^m c_k \phi_k(x_i) = 0 \quad i = 0, 1, \dots, n. \quad (1.6)$$

Consequently, any multiple of the c_k can be added to the α_k without changing the sum of squares of the residuals. Detecting and appropriate handling of such dependence and nonuniqueness constitutes a significant task in the least squares data fitting.

Therefore, taking into account the derivatives as follows

$$\frac{\partial r^2}{\partial \alpha_k} = 0, \quad k = 0, 1, \dots, m \quad (1.7)$$

and interchanging orders of summation, we result in

$$\sum_{k=0}^m \alpha_k \left[\sum_{i=0}^n \phi_k(x_i) \phi_r(x_i) \right] = \sum_{i=0}^n \phi_r(x_i) f(x_i), \quad (1.8)$$

$m + 1$ simultaneous linear equations in $m + 1$ unknown parameters $\alpha_0, \alpha_1, \dots, \alpha_m$, which are the normal equations. The following linear system is derived from the equation

$$\begin{aligned} \alpha_0 \phi_0(x_0) + \alpha_1 \phi_1(x_0) + \dots + \alpha_m \phi_m(x_0) &= f(x_0) \\ \alpha_0 \phi_0(x_1) + \alpha_1 \phi_1(x_1) + \dots + \alpha_m \phi_m(x_1) &= f(x_1) \\ \dots & \\ \alpha_0 \phi_0(x_n) + \alpha_1 \phi_1(x_n) + \dots + \alpha_m \phi_m(x_n) &= f(x_n). \end{aligned} \quad (1.9)$$

This system has a unique solution in the case when $\{x_i : i = 0, 1, \dots, n\}$ are all different. It can be written in the matrix form as

$$PC = Q, \quad (1.10)$$

where

$$\begin{aligned} p_{kr} &= \sum_{i=0}^n \phi_k(x_i) \phi_r(x_i), \\ q_k &= \sum_{i=0}^n \phi_k(x_i) f(x_i). \end{aligned}$$

It can be shown that the matrix P, which is symmetrical and depends only on the coordinate functions, is positive definite, so no pivoting is required. Also, the matrix of coefficients C is symmetrical.

A fundamental drawback to the use of the normal equations should be noticed. The set of normal equations includes small errors in the coefficients or roundoff errors introduced during the solution, which may lead to large errors in the solution of the set. Hence, it is

crucial the errors in the calculated coefficients be estimated.

However, besides the numerical problems that arise, a serious difficulty is how to choose the basis $\{\phi_i : i = 0, 1, \dots, m\}$ so as to provide a suitable approximation to the data. In Chapter 2, we shall see that the piecewise monotonic method suggests a completely different approximation to data smoothing or fitting.

1.1.2 Piecewise monotonic approximation

Consider a smooth function $f(x)$ which is measured at abscissae $x_1 < x_2 < \dots < x_n$ and measurements $\{\phi_i \approx f(x_i) : i = 1, 2, \dots, n\}$ which contain large uncorrelated errors. Demetriou and Powell proposed a data smoothing method that calculates smoothed values $\{y_i : i = 1, 2, \dots, n\}$ and imposes a prescribed number of sign changes, say $k - 1$, on the first differences of the smoothed values. This condition allows k monotonic sections to the smoothed data, so $k - 1$ is the number of sign changes in the first derivative of $f(x)$.

The method minimizes the sum of squares of residuals ε_i as follows

$$\min \sum_{i=1}^n \varepsilon_i^2 = \min \sum_{i=1}^n (y_i - \phi_i)^2 \quad (1.11)$$

subject to the piecewise monotonicity constraints

$$\begin{aligned} y_{t_{j-1}} &\leq y_{t_{j-1}+1} \leq \dots \leq y_{t_j}, & \text{if } j \text{ is odd} \\ y_{t_{j-1}} &\geq y_{t_{j-1}+1} \geq \dots \geq y_{t_j}, & \text{if } j \text{ is even} \end{aligned} \quad (1.12)$$

where the integers $\{t_j : j = 1, 2, \dots, k\}$, positions of turning points, satisfy the condition

$$1 = t_0 \leq t_1 \leq \dots \leq t_k = n. \quad (1.13)$$

Although there are about $O(n^k)$ combinations of the integer variables $\{t_j : j = 0, 1, \dots, k - 1\}$ in order for the problem to be solved, a dynamic programming method that generates the required fit in only $O(kn^2)$ computer operations was developed by Demetriou and Powell [16].

1.2 Non-linear programming problem and Lagrange multipliers

In this section, we state fundamental conditions that are obtained at the solution of a non-linear programming problem when the variables satisfy equality and inequality constraints. These conditions show the importance of the Lagrangian function and of the Lagrange parameters when feasible changes occur in the constraints.

1.2.1 Non-linear programming problem

Consider the non-linear programming problem minimize the objective function

$$f(\underline{x}), \quad \underline{x} \in \mathbb{R}^n \quad (1.14)$$

subject to the constraints

$$c_i(\underline{x}) \geq 0, \quad i = 1, 2, \dots, m, \quad m < n \quad (1.15)$$

where f and each c_i are real functions of \underline{x} (for a general reference, see, Fletcher [9]). We suppose that all functions are twice continuously differentiable. A vector \underline{x} is called “feasible” if it satisfies the constraints (1.15).

The vector \underline{x}^* is a local solution of the non-linear programming problem, if \underline{x} is feasible and if \underline{x} is in the set

$$S(\underline{x}^*, \rho) = \{\underline{x} : \|\underline{x} - \underline{x}^*\| \leq \rho\}, \quad (1.16)$$

then the inequality

$$f(\underline{x}) \geq f(\underline{x}^*)$$

is satisfied.

Suitable conditions are well known in the case when there are no constraints on the variables. Specifically, if \underline{x}^* is a local solution, then the gradient vector $\nabla f(\underline{x}^*)$ is zero and the second derivative matrix $\nabla^2 f(\underline{x}^*)$ is positive definite or positive semi-definite. Conversely, if $\nabla f(\underline{x}^*)$ is zero and if $\nabla^2 f(\underline{x}^*)$ is positive definite, then \underline{x}^* is a local solution (see, Powell [11]).

It is straightforward to extend these definition to the case when all the constraints on \underline{x}

are only the equality constraints (see, for example, Walsh [10])

$$c_i(\underline{x}) = 0, \quad i = 1, 2, \dots, m \quad (1.17)$$

provided that the constraints gradients

$$\{\nabla c_i(\underline{x}^*) : i = 1, 2, \dots, m\}$$

are linearly independent, as we show in the next section.

1.2.2 First order conditions for equality constraints

If the constraints on \underline{x} , are given by (1.17), i.e. all equality constraints, then \underline{x} is a local solution of the non-linear programming problem if the vector $\nabla f(\underline{x}^*)$ and $\{\nabla c_i(\underline{x}) : i = 1, 2, \dots, m\}$ are linearly dependent. Specifically, the Lagrangian condition hold. Namely, if \underline{x}^* is a local solution and if the only constraints are linear equality constraints, then there exist multipliers $\{\lambda_i : i = 1, 2, \dots, m\}$, such that the equation

$$\nabla f(\underline{x}^*) = \sum_{i=1}^m \lambda_i \nabla c_i(\underline{x}^*) \quad (1.18)$$

is satisfied [11].

The assumption that constraint gradients are linearly independent at the solution \underline{x}^* implies that the exist unique values of the Lagrange multipliers $\{\lambda_i : i = 1, 2, \dots, m\}$ such that the equation (1.18) holds. We note that this equation implies that the Lagrangian function

$$L(\underline{x}, \underline{\lambda}) = f(\underline{x}) - \underline{\lambda}^T \underline{c}(\underline{x}) \quad (1.19)$$

is stationary at \underline{x}^* . An interesting interpretation of the Lagrange multipliers is given below [11].

We assume at the moment that equation (1.17) become

$$c_i(\underline{x}) = \underline{b}_i, \quad i = 1, 2, \dots, m. \quad (1.20)$$

Then (1.19) becomes

$$\Psi(\underline{x}, \underline{\lambda}) = f(\underline{x}) - \underline{\lambda}^T (\underline{c}(\underline{x}) - \underline{b}). \quad (1.21)$$

From (1.21) we deduce the interesting result

$$\nabla_{\underline{b}} \Psi(\underline{x}, \underline{\lambda}) = \frac{\partial \Psi(\underline{x}, \underline{\lambda})}{\partial \underline{b}} = \underline{\lambda} \quad (1.22)$$

or

$$\frac{\partial \Psi(\underline{x}, \underline{\lambda})}{\partial b_i} = \lambda_i \quad i = 1, 2, \dots, m. \quad (1.23)$$

This provides an interpretation of the Lagrange multiplier λ_i as a number measuring the marginal potential change in $\Psi(\underline{x}, \underline{\lambda}) = f(\underline{x})$, when b_i is changed by a small amount. Here, of course, we assume that $\underline{x} = \underline{x}^*$. It is of great importance that the implication of (1.23) is deeply understood. The same result is obtained in a different way. Suppose that the right-hand side of (1.20), i.e. the vector \underline{b} , is changed a little by amounts given by the vector

$$\partial \underline{b} = \begin{bmatrix} \partial b_1 \\ \partial b_2 \\ \vdots \\ \partial b_m \end{bmatrix}. \quad (1.24)$$

Then the vector \underline{x} has to change by a vector $\underline{\delta}$ say, such that $\underline{x} + \underline{\delta}$ satisfy the constraints (1.20)

$$c_i(\underline{x} + \underline{\delta}) = b_i + \partial b_i, \quad (1.25)$$

where $\|\underline{\delta}\|$ is small.

We seek an estimate of the change $\{f(\underline{x}^* + \underline{\delta}) - f(\underline{x}^*)\}$ that is caused by the change in the constraints. Even though that there may be much freedom in $\underline{\delta}$ after the constraints are satisfied, we have the very useful property that the Lagrangian condition (1.18) provides a first order estimate of the change to the objective function. Because the constraint conditions give the approximations

$$\begin{aligned} b_i &= c_i(\underline{x}^* + \underline{\delta}) \\ &= c_i(\underline{x}^*) + \underline{\delta}^T \nabla c_i(\underline{x}^*) + O(\|\underline{\delta}\|^2) \\ &= \underline{\delta}^T \nabla c_i(\underline{x}^*) + O(\|\underline{\delta}\|^2) \quad i = 1, 2, \dots, m, \end{aligned} \quad (1.26)$$

where \underline{x}^* is a local solution of the equality constrained problem, we deduce the estimate

$$\begin{aligned}
f(\underline{x}^* + \underline{\delta}) - f(\underline{x}^*) &= \underline{\delta}^T \nabla f(\underline{x}^*) + O(\|\underline{\delta}\|^2) \\
&= \underline{\delta}^T \sum_{i=1}^m \lambda_i \nabla c_i(\underline{x}^*) + O(\|\underline{\delta}\|^2) \\
&= \sum_{i=1}^m \lambda_i b_i + O(\|\underline{\delta}\|^2). \tag{1.27}
\end{aligned}$$

Thus the Lagrange multiplier λ_i is just a multiplier factor in the change to the objective function that occurs if the right-hand side of the constraint $c_i(\underline{x}) = 0$ is altered from zero to b_i .

1.2.3 Quadratic objective function and linear equality constraints

In this section, we replace the general objective function $f(\underline{x})$ by a quadratic function and obtain analogous conditions to (1.27). Consider next the problem of minimizing the objective function

$$Q(\underline{x}) = \underline{\alpha}^T \underline{x} + \frac{1}{2} \underline{x}^T B \underline{x}, \tag{1.28}$$

subject to the $m < n$ linear equality constraints

$$\underline{c}_i^T \underline{x} = 0 \quad i = 1, 2, \dots, m, \tag{1.29}$$

where $\underline{x} \in \mathbb{R}^n$, $\underline{\alpha} \in \mathbb{R}^n$, $\underline{c}_i \in \mathbb{R}^n$ and B is a positive definite $n \times n$ matrix. As usual, the constraint gradients are linearly independent (see, Boot [8]).

The Lagrangian function (1.19) now takes the form

$$\Phi(\underline{x}, \underline{\lambda}) = Q(\underline{x}) - \underline{\lambda}^T C^T \underline{x}, \tag{1.30}$$

where C is the $n \times m$ matrix of the constraints $\underline{c}_i = 1, 2, \dots, m$ and the minimizing procedure again amounts to the taking the first order partial derivatives with respect to \underline{x} and $\underline{\lambda}$ and then equating the results to zero. This gives the system of the $n + m$ equations

$$\underline{\alpha} + B \underline{x} - C \underline{\lambda} = \underline{0} \tag{1.31}$$

$$C^T \underline{x} = \underline{0}. \tag{1.32}$$

If we change the right-hand side of (1.29) from zero to b_i ,

$$\underline{c}_i^T \underline{x} = b_i \quad i = 1, 2, \dots, m, \quad (1.33)$$

equation (1.32) becomes

$$\underline{C}^T \underline{x} = \underline{b}. \quad (1.34)$$

But from (1.30) we deduce for this case as well that (1.22) and (1.23) hold, while (1.25) gives

$$\underline{c}_i^T (\underline{x} + \underline{\delta}) = b_i + \partial b_i \quad (1.35)$$

or for all i ,

$$\underline{C}^T (\underline{x} + \underline{\delta}) = \underline{b} + \partial \underline{b}. \quad (1.36)$$

Hence

$$\underline{C}^T \underline{\delta} = \partial \underline{\delta} \quad (1.37)$$

The vector $\underline{\delta}$ of changes in the components of \underline{x} is not fully determined by $\partial \underline{b}$, because the system $\underline{C}^T \underline{\delta} = \partial \underline{\delta}$ has m equations in n unknowns $m < n$. Now by neglecting terms of second order of magnitude, we have

$$\begin{aligned} \partial f &= f(\underline{x} + \underline{\delta}) - f(\underline{x}) \\ &= (\underline{\alpha} + \underline{B}\underline{x})^T \underline{\delta}, \end{aligned} \quad (1.38)$$

where for uniformity of notation we let $f(\underline{x}) = Q(\underline{x})$.

Next suppose that we are at a minimum point. Thus the equation (1.31) is satisfied and we obtain from (1.38) the equation

$$(\underline{\alpha} + \underline{B}\underline{x} - \underline{C}\underline{\lambda})^T \underline{\delta} = 0. \quad (1.39)$$

Substituting (1.39) into (1.28) and, in view of (1.27), by using

$$\underline{\lambda}^T \underline{C}^T \underline{\delta} = \underline{\lambda}^T \partial \underline{b},$$

we obtain

$$\partial f = \underline{\lambda}^T \partial \underline{b} = \sum_{i=1}^m \lambda_i \partial b_i$$

or

$$\frac{\partial f}{\partial b} = \underline{\lambda}.$$

Thus, as long as we are in a minimum point, a small change ∂b_i in the component b_i changes the value of f by an amount λ_i . The m values of the Lagrangian multipliers are associated with the m constraints, one multiplier for each constraint. The sign of the multiplier is particularly important.

If the sign is positive, a unit increase in b_i is positively valued. One would obtain a smaller value of the objective function if more of b_i were available. In fact the minimum would, according to the argument given above, decrease by an amount λ_i , which in economics is referred to as the shadow price. If the sign is negative, then a unit less of b_i would decrease the value of the objective function by λ_i . One has too much b_i to be good, and would be willing to pay up to λ_i to get rid of one unit b_i . The special case when $\lambda_i = 0$ means that one has the right amount of b_i available. The minimization of the objective function subject to $C^T \underline{x} = \underline{b}$ leads to the same result $\hat{\underline{x}}$, say, whether $\underline{c}_i^T \underline{x} = b_i$ is present or not. That is, if we disregard the constraint $\underline{c}_i^T \underline{x} = b_i$, if we do not impose it, and then proceed to minimize the objective function subject to the remaining constraints we obtain a solution $\hat{\underline{x}}$ which happens to be such that

$$\underline{c}_i^T \hat{\underline{x}} = b_i.$$

This is a degenerate constraint and we are at degeneracy when it occurs (see, for example, [8] and [9]).

1.2.4 First order conditions for inequality constraints

In this section we admit both equality and inequality constraints on the vector of variables, thus we consider the general non-linear problem of section 1.2.1. We consider the case when the vectors $c_i(\underline{x})$, $i = 1, 2, \dots, m$, are linearly independent. If \underline{x}^* is a local minimum, then it is also a local minimum of the problem of minimizing $f(\underline{x})$ subject to the equality conditions

$$c_i(\underline{x}) = 0, \quad i \in E, \quad (1.40)$$

where E is a subset of the constraints indices $\{1, 2, \dots, m\}$. It follows that the first order conditions are

$$\nabla f(\underline{x}^*) = \sum_{i \in E} \lambda_i \nabla c_i(\underline{x}^*), \quad (1.41)$$

where the values of the multipliers are uniquely determined because the constraint gradients are linearly independent. Further, the remarks of the last paragraph of section 1.2.2 show that, if λ_i is negative, then the objective function can be reduced by changing \underline{x}^* by a small amount, so that the constraint function $c_i(\underline{x})$ becomes positive, which preserves feasibility. Therefore, if \underline{x}^* is a local solution to the main non-linear programming problem, then not only is $\nabla f(\underline{x}^*)$ in the linear space spanned by the vectors

$$\{\nabla c_i(\underline{x}^*) : i \in E\},$$

but also the multipliers $\{\lambda_i : i \in E\}$ in expression (1.41) are nonnegative. This is stated by the following fundamental theorem [9].

Theorem (Karush-Kuhn-Tucker conditions).

If \underline{x}^* is a local solution of the problem that minimizes the objective function (1.14) subject to (1.15), then there exist multipliers $\{\lambda_i : i \in E\}$, where

$$\lambda_i \geq 0 \quad i \in E$$

and

$$\lambda_i = 0 \quad i \in \{1, 2, \dots, m\} \setminus E,$$

such that the gradient of the objective function at \underline{x}^* has the form

$$\nabla f(\underline{x}^*) = \sum_{i \in E} \lambda_i \nabla c_i(\underline{x}^*). \quad \square \quad (1.42)$$

It follows from this theorem that

$$\lambda_i = 0 \quad \text{if } c_i(\underline{x}^*) > 0, \quad i \in \{1, 2, \dots, m\} \setminus E.$$

Thus, if there exist multipliers $\{\lambda_i : i \in E\}$ that satisfy equation (1.42) and the conditions

$$\begin{aligned}\lambda_i &\geq 0 \quad i \in E \\ \lambda_i &= 0, \quad c_i(\underline{\mathbf{x}}^*) > 0\end{aligned}\tag{1.43}$$

then $\underline{\mathbf{x}}^*$ is a Karush-Kuhn-Tucker points. These points correspond to stationary points of the objective function when there are no constraints, because any more away from a Karush-Kuhn-Tucker point that maintains feasibility and that reduces the objective function can only reduce the objective function by an amount that is of second order in the change of variables. Specifically, if $\underline{\mathbf{d}}$ is small and if $(\underline{\mathbf{x}}^* + \underline{\mathbf{d}})$ is feasible, then expressions (1.42) and (1.43) imply the band

$$\begin{aligned}f(\underline{\mathbf{x}}^* + \underline{\mathbf{d}}) - f(\underline{\mathbf{x}}^*) &= \underline{\mathbf{d}}^T \nabla f(\underline{\mathbf{x}}^*) + O(\|\underline{\mathbf{d}}\|^2) \\ &= \underline{\mathbf{d}}^T \sum_{i \in E} \lambda_i \nabla c_i(\underline{\mathbf{x}}^*) + O(\|\underline{\mathbf{d}}\|^2) \\ &= \sum_{i \in E} \lambda_i \underline{\mathbf{d}}^T \nabla c_i(\underline{\mathbf{x}}^*) + O(\|\underline{\mathbf{d}}\|^2) \\ &= \sum_{i \in E} \lambda_i [c_i(\underline{\mathbf{x}}^* + \underline{\mathbf{d}}) - c_i(\underline{\mathbf{x}}^*)] + O(\|\underline{\mathbf{d}}\|^2) \\ &\geq O(\|\underline{\mathbf{d}}\|^2),\end{aligned}$$

where the penultimate equality follows from the first order approximation to the constraint functions.

Thus, any feasible change to a local solution is bounded below by a second order change to the objective function [11].

Chapter 2

Piecewise monotonic data approximation

2.1 Definition of piecewise monotonic data approximation

The piecewise monotonic data approximation is a data smoothing method. Introduced by Demetriou and Powell [16] and it provides some useful applications in image processing, signal restoration and spectroscopy(see, for example, [3] and [18]). This method has some significant advantages over others currently used smoothing methods. The method is particularly suitable when the errors are large and uncorrelated and choosing a set of approximation functions is not needed. Also, the smoothing process is a projection because, if it is applied to smoothed data, then there is no need for changes.

Let n, k be positive integers, where n is the number of data and k is a prescribed integer, such that $k < n$ and let $\{\phi_i = \phi(x_i) : i = 1, 2, \dots, n\}$ be a sequence of measured values of a signal $f(x)$ at the abscissae $x_1 < x_2 < \dots < x_n$. The measurements contain uncorrelated random errors (noise) ε_i such that $\phi(x_i) = f(x_i) + \varepsilon_i$. We assume that if the signal has turning points, their number is much lower than the number of measurements. Also, let $\{y_i : i = 1, 2, \dots, n\}$ be a sequence of smoothed values. Some algorithms have been developed by Demetriou & Powell [16] and also by Demetriou [13] and [14] that modify the measurements if their first differences $\{y_{i+1} - y_i : i = 1, 2, \dots, n-1\}$ contain more than $k-1$ sign changes. This is a condition that allows k monotonic sections to the smoothed data.

We regard $\{\phi_i : i = 1, 2, \dots, n\}$ as components of n -vector $\underline{\phi}$, $\{y_i : i = 1, 2, \dots, n\}$ as components of n -vector \underline{y} and for the present that k is known. The method [16] calculates

a vector \underline{y} that minimizes the sum of squares of the errors

$$\Phi(\underline{y}) = \sum_{i=1}^n (y_i - \phi_i)^2 \quad (2.1)$$

subject to the piecewise monotonicity constraints

$$\begin{aligned} y_{t_{j-1}} &\leq y_{t_{j-1}+1} \leq \cdots \leq y_{t_j}, & \text{if } j \text{ is odd} \\ y_{t_{j-1}} &\geq y_{t_{j-1}+1} \geq \cdots \geq y_{t_j}, & \text{if } j \text{ is even} \end{aligned} \quad (2.2)$$

where $\{t_j : j = 0, 1, \dots, k\}$ are integers, that is to say the positions of the turning points or extrema of the fit, satisfy the conditions

$$1 = t_0 \leq t_1 \leq \cdots \leq t_k = n. \quad (2.3)$$

The integers $\{t_j : j = 1, 2, \dots, k-1\}$ which not known originally, are variables in the optimization calculation that gives a best fit. While the number of combinations of integer variables is raised to the order $O(n^k)$, the piecewise monotonic approximation method allows an efficient and automatic calculation of an optimal fit \underline{y} in only $O(kn^2)$ computer operations. Especially, when $k = 1$ or $k = 2$, this complexity reduces to $O(n)$.

When the number of extrema in the data is less than $k-1$, $\underline{\phi}$ satisfies the piecewise monotonicity constraints, so $\underline{y} = \underline{\phi}$. On the contrary the case of \underline{y} not satisfying the piecewise monotonicity constraints, the turning point indices $\{t_j : j = 1, 2, \dots, k-1\}$ are all different. At the turning points of a best fit \underline{y} , we have the interpolation conditions

$$y_{t_j} = \phi_{t_j} \quad j = 1, 2, \dots, k-1. \quad (2.4)$$

Each monotonic section in a best piecewise monotonic fit can be obtained by a separate calculation, since it is the optimal fit itself to the corresponding data. The components $\{y_i : i = t_{j-1}, t_{j-1} + 1, \dots, t_j\}$ on $[x_{t_{j-1}}, x_{t_j}]$ minimize the sum of squares

$$\sum_{i=t_{j-1}}^{t_j} (y_i - \phi_i)^2 \quad (2.5)$$

subject to the constraints

$$y_i \leq y_{i+1} \quad i = t_{j-1}, \dots, t_j - 1, \quad \text{if } j \text{ is odd} \quad (2.6)$$

or subject to the constraints

$$y_i \geq y_{i+1} \quad i = t_{j-1}, \dots, t_j - 1, \quad \text{if } j \text{ is even,} \quad (2.7)$$

which is a strictly convex quadratic programming problem with a unique solution. In the former case the sequence $\{y_i : i = t_{j-1}, t_{j-1} + 1, \dots, t_j\}$ is the best monotonic increasing fit to $\{\phi_i : i = t_{j-1}, t_{j-1} + 1, \dots, t_j\}$. Respectively, in the latter case it is the best decreasing fit. Therefore, under the condition that $\{t_j : j = 1, 2, \dots, k - 1\}$ are known, solving a separate monotonic problem on each section $[x_{t_{j-1}}, x_{t_j}]$ is required to calculate the components of \underline{y} .

2.2 The monotonic problem

The monotonic increasing problem seeks a vector \underline{y} in \mathbb{R}^n that minimizes the sum of squares of the errors, defined by (2.1), subject to the monotonic constraints

$$y_1 \leq y_2 \leq \dots \leq y_n. \quad (2.8)$$

This problem appeared first by van Eeden [17] in 1956, and since then many publications have appeared because it has many applications in statistics, operations and operation research, for instance. It is a strictly quadratic programming problem (see, [9]) because the Hessian matrix of the objective function with respect to \underline{y} is twice the unit matrix and the constraints on \underline{y} are linear. Therefore, it has a unique solution.

Several algorithms are available, but in our method we use the algorithm of Demetriou & Powell (1991) which is suited to the problem and is very efficient. To be specific, the algorithm is based on van Eeden's method and generates a sequence of estimates of the solution. Initially, it sets $\underline{y} = \underline{\phi}$, so it relaxes all the constraints (2.8) and subsequently any violated constraint is satisfied as an equation. The process finishes when all constraints are considered and also makes some backtracking to avoid possible constraint violations for the estimates. The most important feature of this approach is that we can obtain the best monotonic approximation in only $O(n)$ operations.

The following example gives the best approximation to data from $\sin(\pi x) + \varepsilon_i$, $x \in [0, 0.5]$ at equally spaced abscissae, when $\varepsilon_i \sim U[-1, 1]$. Figure 2.1 illustrates the best monotonic increasing approximation. We see that the components are piecewise constants on the intervals $[1, 2] \cup [3, 4] \cup [5, 17] \cup [18, 28] \cup [29, 35] \cup [36, 40]$.

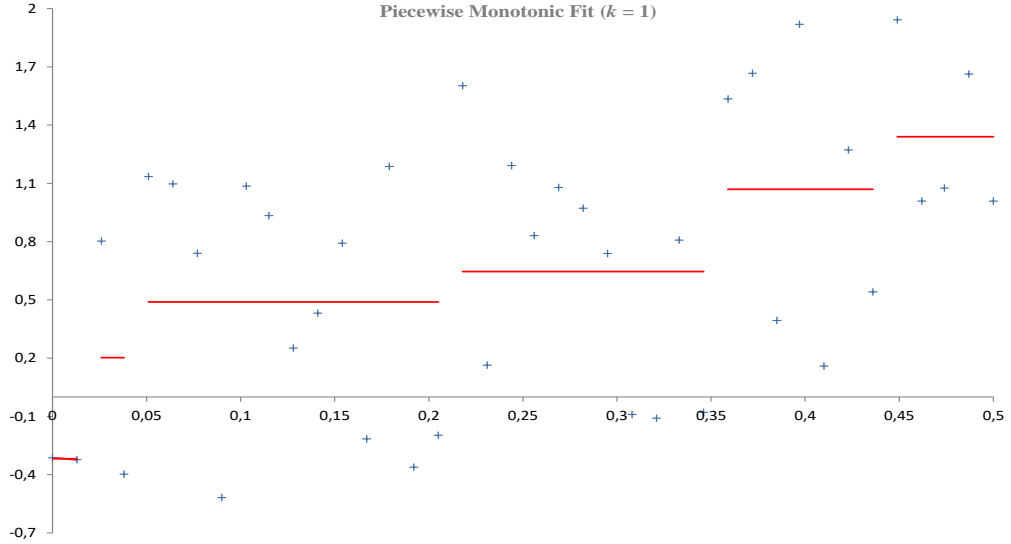


Figure 2.1: Graphical representation of the data given in Table 2.1. Best monotonic fit with $k = 1$ to 40 data points (plus signs) of $\sin(\pi x) + \varepsilon_i$. The solid line illustrates the best fit.

The best monotonic decreasing approximation is tested as the increasing one if the order of the data is reversed. We feed the data to L2WPMA with $k = 1$ and obtain the results we present in Table 2.1.

Table 2.1: Best fits with $k = 1$ monotonic sections to measurements of $\sin(\pi x) + \varepsilon_i$

i	x_i	ϕ_i	y_i	Δy_i	λ_i	i	x_i	ϕ_i	y_i	Δy_i	λ_i
1	0.000	-0.313	-0.318	-	-	21	0.256	0.831	0.646	0.000	2.040
2	0.013	-0.323	-0.318	0.000	0.010	22	0.269	1.079	0.646	0.000	2.409
3	0.026	0.803	0.203	-0.521	0.000	23	0.282	0.972	0.646	0.000	3.274
4	0.038	-0.397	-0.203	0.000	1.200	24	0.295	0.739	0.646	0.000	3.926
5	0.051	1.135	0.489	-0.286	0.000	25	0.308	-0.090	0.646	0.000	4.111
6	0.064	1.097	0.489	0.000	1.291	26	0.321	-0.109	0.646	0.000	2.638
7	0.077	0.740	0.489	0.000	2.506	27	0.333	0.808	0.646	0.000	1.127
8	0.090	-0.518	0.489	0.000	3.007	28	0.346	-0.079	0.646	0.000	1.451
9	0.103	1.086	0.489	0.000	0.992	29	0.359	1.535	1.070	-0.423	0.000
10	0.115	0.934	0.489	0.000	2.185	30	0.372	1.667	1.070	0.000	0.931
11	0.128	0.252	0.489	0.000	3.074	31	0.385	0.394	1.070	0.000	2.126
12	0.141	0.432	0.489	0.000	2.600	32	0.397	1.919	1.070	0.000	0.775
13	0.154	0.792	0.489	0.000	2.485	33	0.410	0.159	1.070	0.000	2.473
14	0.167	-0.216	0.489	0.000	3.090	34	0.423	1.272	1.070	0.000	0.652
15	0.179	1.187	0.489	0.000	1.679	35	0.436	0.541	1.070	0.000	1.057
16	0.192	-0.361	0.489	0.000	3.074	36	0.449	1.942	1.340	-0.270	0.000
17	0.205	-0.197	0.489	0.000	1.373	37	0.462	1.009	1.340	0.000	1.204
18	0.218	1.603	0.646	-0.157	0.000	38	0.474	1.076	1.340	0.000	0.543
19	0.231	0.164	0.646	0.000	1.913	39	0.487	1.663	1.340	0.000	0.015
20	0.244	1.192	0.646	0.000	0.949	40	0.500	1.009	1.340	0.000	0.662

2.3 Lagrange multipliers in the monotonic case

In this section we state how the Lagrange multipliers are calculated by the piecewise monotonic approximation, although they are not required for obtaining the optimal fit (see, [14]).

Consider $\{\lambda_i : i = 2, 3, \dots, n\}$ as the Lagrange multipliers. Also consider $\{t_i : i = 1, 2, \dots, k-1\}$ as the optimal sequence of integers and the associated optimal fit \underline{y} which have been obtained. Let E be a subset of the active constraint indices $\{2, 3, \dots, n\}$, such that $E = \{i : y_{i-1} - y_i = 0\}$.

The Karush-Kuhn-Tucker conditions for the problem that minimizes the objective function (2.1) subject to (2.2) lead to

$$\text{grad } \Phi(\underline{y}) = \sum_{i \in E} \lambda_i (e^{i-1} - e^i), \quad (2.9)$$

where e^i is the i th coordinate vector in \mathbb{R}^n . The Lagrange multipliers $\{\lambda_i : i \in E\}$ are nonnegative in the increasing case, when $i \in [2, t_1] \cap E$ and $i \in [t_{j-1} + 1, t_j] \cap E$ for j odd, and respectively they are nonpositive in the decreasing case, when $i \in [t_{j-1} + 1, t_j] \cap E$ for j even. Essentially, the Lagrange multipliers of the piecewise monotonic approximation case alternate in the sign along with the intervals $[t_0, t_1]$, $[t_1, t_2]$, and so on of optimal integer variables. Furthermore, they are equal to zero $\lambda_i = 0$ for all integers i in $[2, n]$, so that $\underline{\lambda}$ is a $(n-1)$ -vector.

The Lagrange multipliers are calculated due to the equations in E that the components of \underline{y} occur in ranges of values on which they are equal. Without loss of generality we assume that j is an odd integer in $[1, k]$. We regard $\{y_i : i = t_{j-1}, \dots, t_j\}$ as the best monotonic increasing approximation to $\{\phi_i : i = t_{j-1}, \dots, t_j\}$ and s and t any integers such that $t_{j-1} \leq s < t \leq t_j$. Considering the above, $\{\lambda_i : i = s+1, s+2, \dots, t\}$ satisfy the following relations

$$\begin{aligned} 2(y_s - \phi_s) &= -\lambda_{s+1} \\ 2(y_{s+1} - \phi_{s+1}) &= \lambda_{s+1} - \lambda_{s+2} \\ &\dots \\ 2(y_{t-1} - \phi_{t-1}) &= \lambda_{t-1} - \lambda_t \\ 2(y_t - \phi_t) &= \lambda_t \end{aligned} \quad (2.10)$$

We let η_{st} be the value that minimizes the expression $\sum_{i=s}^t (\eta - \phi_i)^2$ and by a straightforward calculation we obtain

$$\eta_{st} = \frac{1}{t-s+1} \sum_{i=s}^t \phi_i$$

In the case that $y_s = y_{s+1} = \dots = y_t$, $s = t_{j-1}$ or $y_{s-1} < y_s$ and $t = t_j$ or $y_t < y_{t+1}$, it follows that $y_s = \eta_{st}$. As a result the Lagrange multipliers can be calculated recursively by equations (2.10) in only $O(t-s)$ computer operations as follows

$$\begin{aligned} \lambda_{s+1} &= -2(\eta_{st} - \phi_s) \\ \lambda_{s+2} &= \lambda_{s+1} - 2(\eta_{st} - \phi_{s+1}) \\ &\dots \\ \lambda_t &= \lambda_{t-1} - 2(\eta_{st} - \phi_{t-1}). \end{aligned} \tag{2.11}$$

Since Lagrange multipliers came from the solution of a quadratic programming problem, they have the properties that have been given in the quadratic programming case, which has been studied in chapter 1.

We use the data of the example of section 2.2, we calculate the Lagrange multipliers and present their values in Table 2.1. As we expected about the Karush-Kuhn-Tucker conditions all λ_i are nonnegative. We note that in our example λ_i are zero for i such that $y_{i-1} = y_i$.

Chapter 3

Experimental Results

In this chapter we perform experiments to study how the Lagrange multipliers are changed as the number of monotonic sections in a piecewise monotonic approximation is changed.

3.1 Setting the experiment

In order to present the behavior of Lagrange multipliers λ_i when the number of monotonic sections k increases, we have to define those measures that present important information about this correlation.

For this purpose, we will use nine Raman spectrum datafiles, eight datafiles of mineral which are downloaded from Laboratory of Photoinduced Effects Vibrational and X-RAY Spectroscopies, a freely available database on the website [25], of the Department of Physics, University of Parma, and one datafile of carbohydrate which is downloaded from SPECARB, a freely available database on the website [27], of the Department of Food Science, Faculty of Science, University of Copenhagen. In addition, we will use a MS spectrum datafile of thyroid hormone which is downloaded from Human Metabolome Database, a freely available electronic database on [26], supported by the Canadian Institutes of Health Research, Canada Foundation for Innovation, and by The Metabolomics Innovation Centre.

L2WPMA, as we have mentioned, calculates a least squares piecewise approximation to univariate data which contain random errors. The datafiles consist of two-column data, where the first column keeps the Raman shift, providing the values $\{x_i : i = 1, 2, \dots, n\}$ as the abscissae, which are irrelevant to the calculation, and the second column keeps the intensity, providing the values $\{\phi_i : i = 1, 2, \dots, n\}$. The method supplies the smoothed

data of the best fit $\{y_i : i = 1, 2, \dots, n\}$, the positions of the turning points of the best fit $\{t_j : j = 1, 2, \dots, k-1\}$, the value of the objective function and the Lagrange multipliers, one multiplier for each constraint, which are also irrelevant to the actual calculation of the best fit.

The Lagrange multipliers are interpreted as rates of change of the objective function (2.1). A possible relaxation of an inactive constraint reduces the value of the objective function (2.1) by an amount equal to the value of the multiplier λ_i . It is known that the nonzero Lagrange multipliers correspond to active constraints, so a sensitivity analysis concludes that the best fit is strongly dependent upon the placement of all active constraints.

Before we state the experiment, it is necessary to define that E is the subset of active constraints indices $\{2, \dots, n\}$, such that $\lambda_i \in E$ are nonzero Lagrange multipliers. We determine that $\mathbb{Y}(k, n)$ is the set of the feasible vectors \underline{y} in \mathbb{R}^n with k monotonic sections increasing and decreasing alternately. Therefore, in this experiment for the optimal \underline{y} in $\mathbb{Y}(k, n)$ we calculate the following measures

1. $SSR = \|\underline{y} - \underline{\phi}\|^2$, the sum of squares of residuals, the value of the objective function, that is the square distance between the smoothed values y_i and the function values ϕ_i , $i = 1, 2, \dots, n$
2. $D = \max_{1 \leq i \leq n} |y_i - \phi_i|$, the maximum estimated error, that is the maximum absolute difference between the smoothed values y_i and the function values ϕ_i , $i = 1, 2, \dots, n$
3. $L = \max_{\lambda_i \in E} |\lambda_i|$, the maximum absolute value of the nonzero Lagrange multipliers, that is of the active constraints
4. $\ell = \min_{\lambda_i \in E} |\lambda_i|$, the minimum absolute value of the nonzero Lagrange multipliers, that is of the active constraints
5. $\log_{10}L$ and $\log_{10}\ell$, the decadic logarithms of the maximum and minimum absolute values of the nonzero Lagrange multipliers

for different values of the monotonic sections k , with the aim of examining how these measures are changed in connection with k .

3.2 The Raman spectrum of zircon

The first Raman spectrum datafile regards mineral zircon. The file contains 1024 pairs of data and is tested for k in $\{1, 2, \dots, 16\}$. We start feeding the data, without any preliminary analysis, to L2WPMA, for $k = 1$, one monotonic section. The best fit and the corresponding Lagrange multipliers, as well as the calculations of the measures which are examined, are far too many to be presented as raw numbers in the pages, so refer to Zicron.xlsx, sheet $k = 1$. Nevertheless, we may capture the main features of the data set by looking at Fig. 3.1. The data are denoted by plus sign “+” and the piecewise linear interpolant to the smoothed values illustrates the fit.

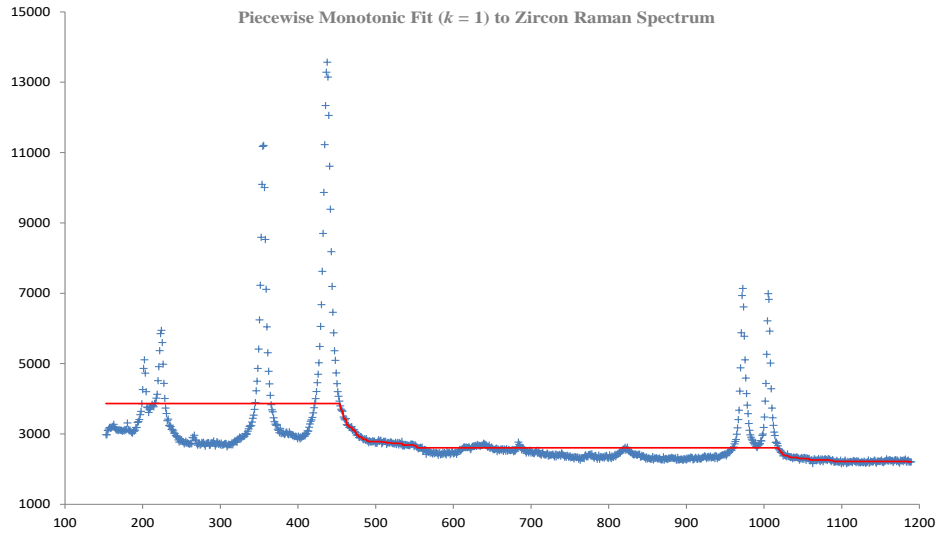


Figure 3.1: Detected peaks (circles) by a best monotonic fit with $k = 1$ to 1024 data points (plus signs) of the zircon Raman spectrum. The solid line illustrates the best fit. The numbers give the intensities at the corresponding Raman shifts.

The measures which we mentioned in section 3.1 can be calculated by the results of the running program. First, the sum of squares of residuals and the maximum absolute value of estimated error are equal to 1.33×10^9 and 9.70×10^3 respectively. Second, the maximum and minimum absolute value of nonzero Lagrange multipliers are equal to 2.42×10^5 and 2.10×10^0 respectively. Last, the corresponding decadic logarithms of the above maximum and minimum values of nonzero Lagrange multipliers are equal to 5.38×10^0 and 3.22×10^{-1} respectively.

The experiment continues for $k = 2$, two monotonic sections. The corresponding best fit and Lagrange multipliers refer to Zicron.xlsx, sheet $k=2$. The data and the best fit for $k = 2$ are displayed in Fig. 3.2. In this case the measures are $SSR = 5.72 \times 10^8$, $D = 7.13 \times 10^3$, $L = 1.40 \times 10^5$, $\ell = 4.20 \times 10^{-1}$, $\log_{10}L = 5.15 \times 10^0$ and $\log_{10}\ell = -3.77 \times 10^{-1}$.

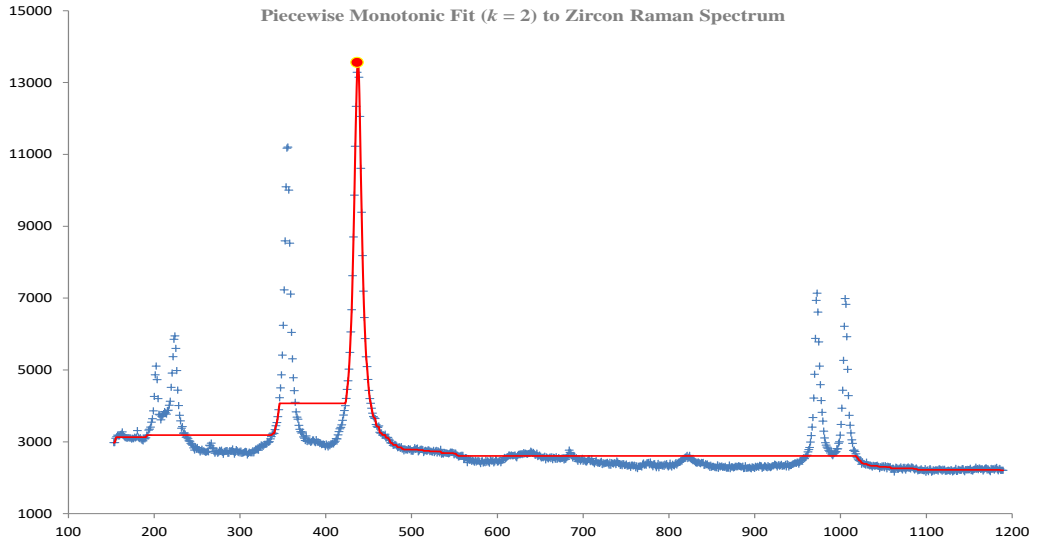


Figure 3.2: As in Fig. 3.1, but detected peaks by a best monotonic fit with $k = 2$. The peak is indicated by circle.

For $k = 3$, three monotonic sections, the results of the running program and the calculations are presented in Zircon.xlsx, sheet $k = 3$. Therefore, the corresponding data and the best fit are displayed in Fig. 3.3. The measures are equal to the case when $k = 2$, except for the sum of squares of residuals, the minimum nonzero Lagrange multipliers and the corresponding decadic logarithms, which are equal to 5.42×10^8 , 2.10×10^0 and 3.22×10^{-1} respectively.

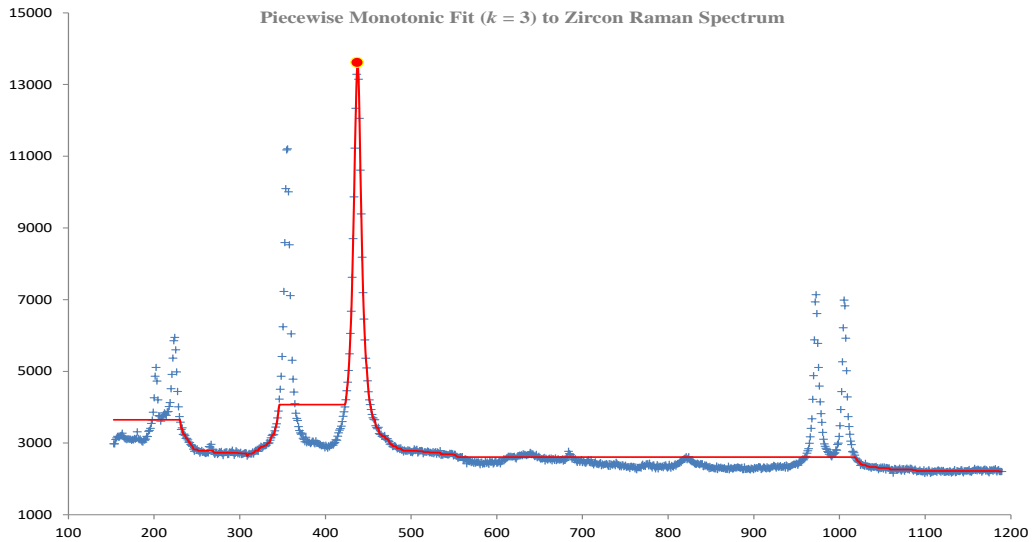


Figure 3.3: As in Fig. 3.1, but detected peaks by a best monotonic fit with $k = 3$. The peak is indicated by circle.

When $k = 4$, four monotonic sections, the results from the running program and the calculations are presented in Zircon.xlsx, sheet 4. The data, the resultant fit and the peaks are shown in Fig. 3.4. The values of measures are $SSR = 2.75 \times 10^8$, $D = 5.43 \times 10^3$, $L = 1.40 \times 10^5$, $\ell = 4.20 \times 10^{-1}$, $\log_{10}L = 5.15 \times 10^0$ and $\log_{10}\ell = -2.73 \times 10^{-1}$.

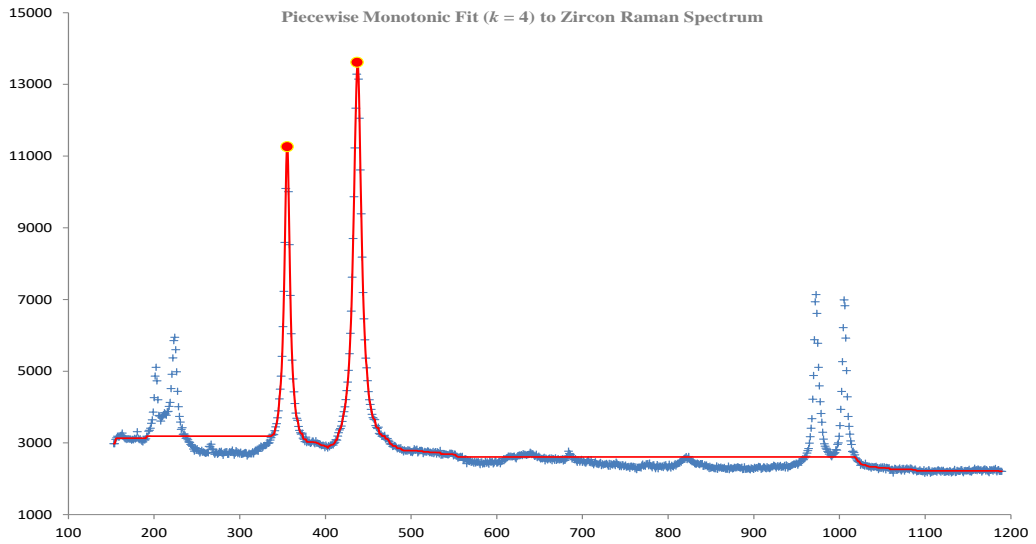


Figure 3.4: As in Fig. 3.1, but detected peaks by a best monotonic fit with $k = 4$. The peaks are indicated by circle.

It is observed that Raman spectrum data sets consist of increasing and decreasing monotonic sections alternately. They start with an increasing monotonic section and end with a decreasing monotonic section. As a result, in this case, the piecewise monotonic approximation detects the most important peaks only when k is even. Despite the fact that we continue to consider all cases for k in $\{5, 6, \dots, 16\}$, we will present only figures in which the piecewise monotonic approximation detects the most important peaks for even monotonic sections. It is usual in practice that the turning points of an optimal fit with k monotonic sections are preserved by the optimal fit with $k + 2$ monotonic sections. However, it should be noted that this depends on the specific calculation and does not necessarily happen generally (see, for example, [12]).

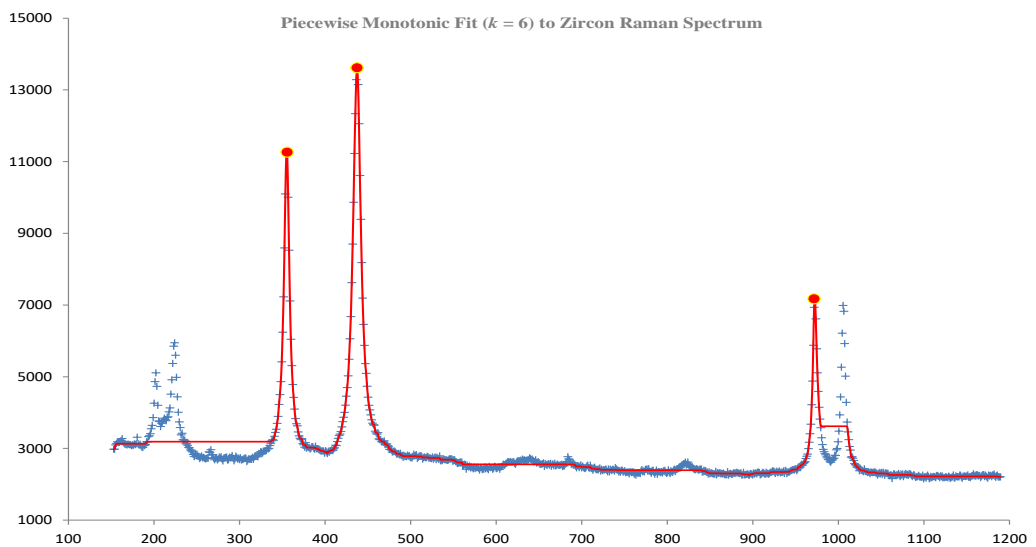


Figure 3.5: As in Fig. 3.1, but detected peaks by a best monotonic fit with $k = 6$. The peaks are indicated by circle.

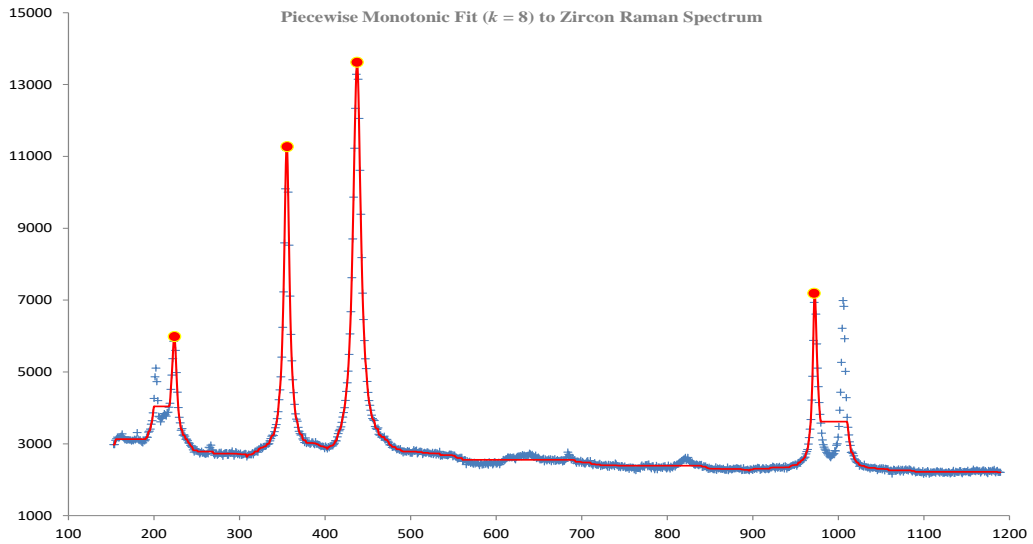


Figure 3.6: As in Fig. 3.1, but detected peaks by a best monotonic fit with $k = 8$. The peaks are indicated by circle.

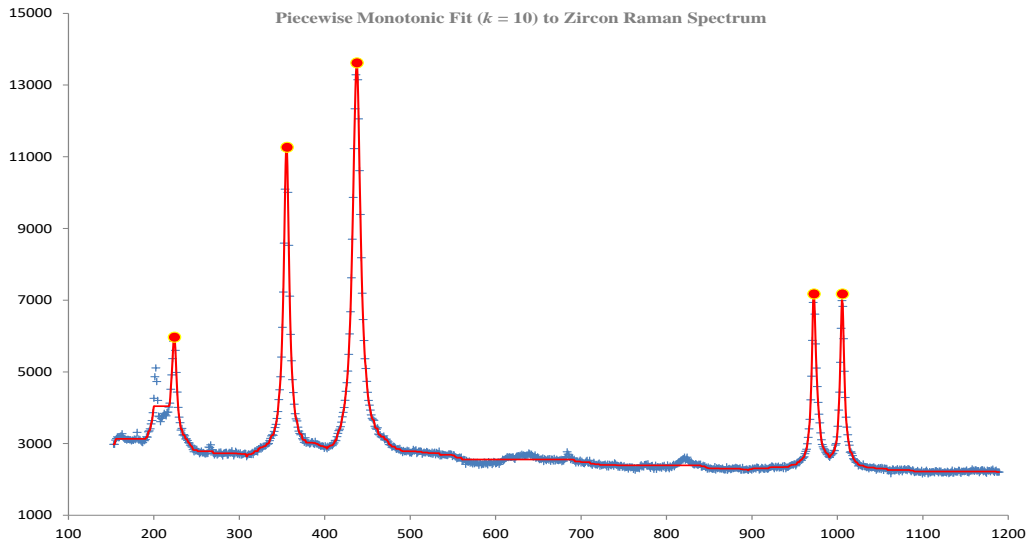


Figure 3.7: As in Fig. 3.1, but detected peaks by a best monotonic fit with $k = 10$. The peaks are indicated by circle.

The piecewise monotonic approximation makes the sum of squares of the residuals smaller, while k increases, maintaining the most important turning points. Having a known underlying function enables us to see whether the fit is more accurate than the measurements and it is. For $k = 12$ the method captures effectively the trends of the data and detects appropriate peaks (see Fig. 3.8). However, we continue increasing the number of monotonic sections k , in which the method detects not so important peaks, in order to examine the behavior of the measures that are mentioned in section 3.1. By increasing the number of sections k , it is observed that the method detects subtle trends in the data, which are not detected for smaller values of k , because they are rather conservative (see Fig 3.9 and 3.10). Therefore, for $k = 16$ the method detects 15 turning points, 8 of which

are peaks.

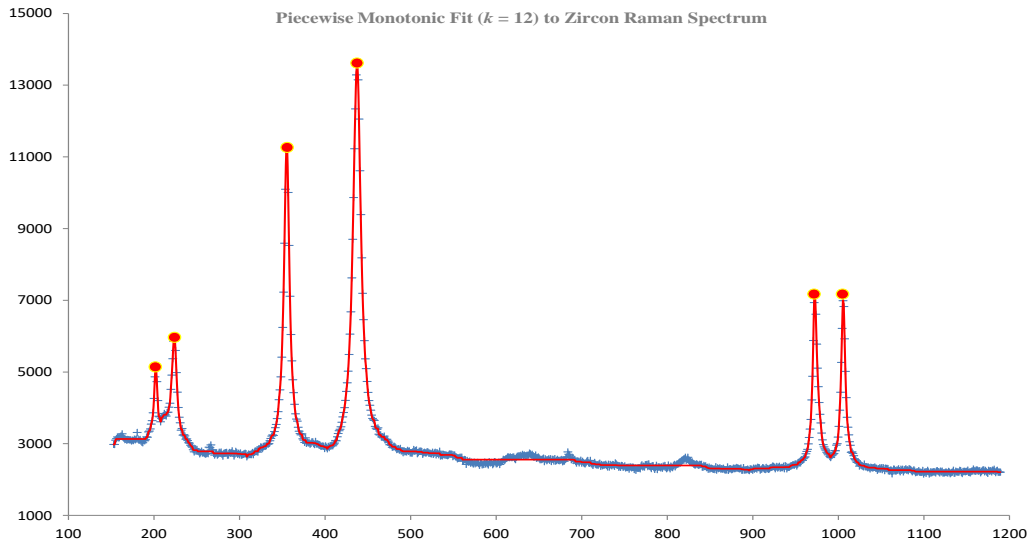


Figure 3.8: As in Fig. 3.1, but detected peaks by a best monotonic fit with $k = 12$. The peaks are indicated by circle.

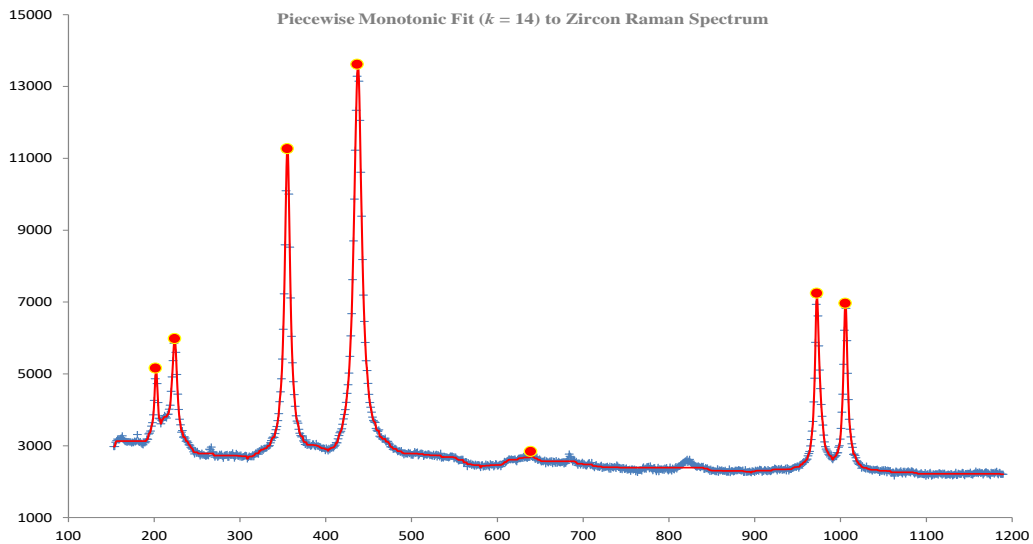


Figure 3.9: As in Fig. 3.1, but detected peaks by a best monotonic fit with $k = 14$. The peaks are indicated by circle.

Thus, following the above procedure, we calculate the best fit and the corresponding Lagrange multipliers, which are presented in Zircon.xlsx with the absolute value of Lagrange multipliers and estimated errors, with L2WPMA. The main features of the data sets may be captured by the figures, when k increases.

The behavior of the approximation is explored by presenting in Table 3.1 the positions of the turning points by piecewise monotonic fits to the zircon data for values of k in $\{2, 4, \dots, 16\}$. In the right part of Table 3.1 we indicate the turning point positions of each optimal fit for k in $\{2, 4, \dots, 16\}$ in correspondence with the column labeled “ t_j ”, derived when $k = 16$. For instance, when $k = 6$ the turning points occur at the positions 188, 232,

265, 716 and 795 as indicated by the times signs in the column labeled “6”. We notice that the extra turning points of the optimal approximation with $k + 2$ monotonic sections occur between adjacent turning points of the optimal approximation with k monotonic sections.

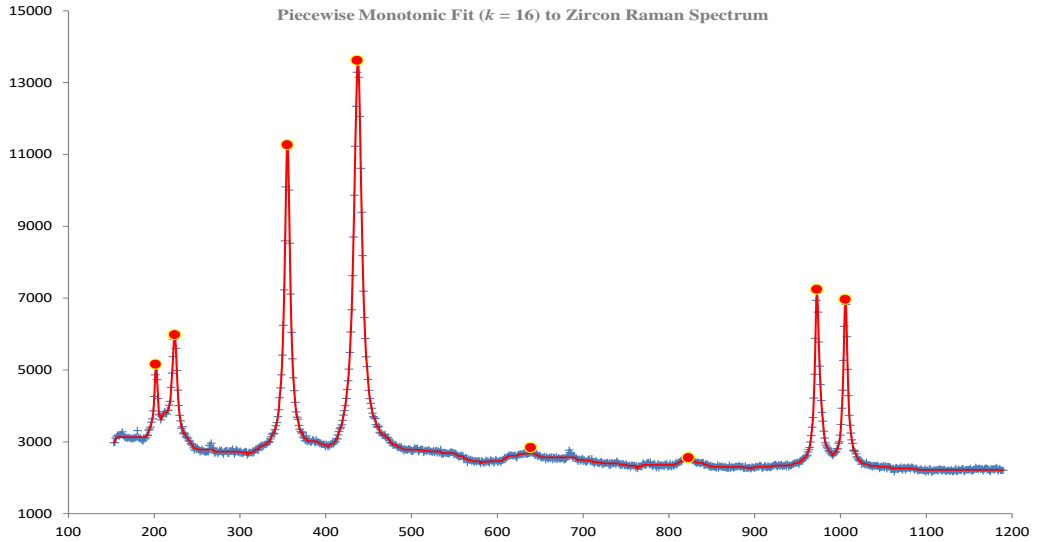


Figure 3.10: As in Fig. 3.1, but detected peaks by a best monotonic fit with $k = 16$. The peaks are indicated by circle.

Table 3.1: Left four columns: Turning points in the zircon spectrum by a best fit with $k = 16$ monotonic sections. Right eight columns: The turning point positions of the optimal fit for k in $\{2, 4, \dots, 16\}$ are indicated by the times sign

j	t_j	x_{t_j}	Intensity (ϕ_{t_j})	$k =$	2	4	6	8	10	12	14	16
0	1	1.53×10^2	2.98×10^3		×	×	×	×	×	×	×	×
1	46	2.02×10^2	5.11×10^3							×	×	×
2	51	2.08×10^2	3.61×10^3							×	×	×
3	66	2.24×10^2	5.95×10^3					×	×	×	×	×
4	144	3.09×10^2	2.64×10^3					×	×	×	×	×
5	188	3.56×10^2	1.12×10^4			×	×	×	×	×	×	×
6	232	4.03×10^2	2.86×10^3			×	×	×	×	×	×	×
7	265	4.38×10^2	1.36×10^4		×	×	×	×	×	×	×	×
8	402	5.80×10^2	2.40×10^3								×	×
9	459	6.39×10^2	2.74×10^3								×	×
10	582	7.63×10^2	2.26×10^3									×
11	643	8.24×10^2	2.62×10^3									×
12	716	8.96×10^2	2.25×10^3				×	×	×	×	×	×
13	795	9.73×10^2	7.14×10^3				×	×	×	×	×	×
14	814	9.91×10^2	2.61×10^3						×	×	×	×
15	829	1.01×10^3	6.99×10^3						×	×	×	×
16	1024	1.19×10^3	2.21×10^3		×	×	×	×	×	×	×	×

In Table 3.2 are displayed the centralized measures of the experiment, which are mentioned in section 3.1 for k monotonic sections, k in $\{1, 2, \dots, 16\}$. It is observed that the sum of squares of residuals decreases while the value of the monotonic sections k increases. More specifically, the order of magnitude of SSR is 10^9 for k in $\{1, 2, \dots, 6\}$ and it decreases to 10^8 from k in $\{7, 8, 9\}$. For k in $\{10, 11, \dots, 15\}$ it falls to 10^6 . For $k = 16$ the order of magnitude falls more to 10^5 . A reduction in the order of magnitude also occurs in the maximum absolute value of estimated errors, as the number of monotonic sections increases. For k in $\{1, 2, \dots, 11\}$ it is equal to 10^3 while for k in $\{12, 13, \dots, 16\}$ it reduces to 2.3×10^2 . The maximum absolute value of nonzero Lagrange multipliers reduces while k increases. More specifically, the order of magnitude starts from 10^5 , for k in $\{1, 2, \dots, 5\}$, decreases to 10^4 , for k in $\{6, 7, 8, 9\}$, and to 10^3 for k in $\{10, 11, \dots, 16\}$. The minimum absolute value of nonzero Lagrange multipliers presents a fluctuation, that is for k in $\{1, 3, 5\}$ the value is 2.1×10^0 and for k in $\{7, 9, 11, 13, 15\}$ is 5.60×10^{-1} , while for k even is equal to 4.20×10^{-1} . Their decadic logarithms have a corresponding behavior.

Table 3.2: Measures for Zircon.

k	SSR	D	L	ℓ	$\log_{10}L$	$\log_{10}\ell$
1	1.33×10^9	9.70×10^3	2.42×10^5	2.10×10^0	5.38×10^0	3.22×10^{-1}
2	5.72×10^8	7.13×10^3	1.40×10^5	4.20×10^{-1}	5.15×10^0	-3.77×10^{-1}
3	5.42×10^8	7.13×10^3	1.40×10^5	2.10×10^0	5.15×10^0	3.22×10^{-1}
4	2.75×10^8	4.53×10^3	1.40×10^5	4.20×10^{-1}	5.15×10^0	-2.73×10^{-1}
5	2.45×10^8	4.53×10^3	1.40×10^5	2.10×10^0	5.15×10^0	3.22×10^{-1}
6	1.24×10^8	3.37×10^3	7.19×10^4	4.20×10^{-1}	4.86×10^0	-3.77×10^{-1}
7	9.34×10^7	3.37×10^3	4.06×10^4	5.60×10^{-1}	4.61×10^0	-2.52×10^{-1}
8	5.82×10^7	3.37×10^3	3.29×10^4	4.20×10^{-1}	4.52×10^0	-3.77×10^{-1}
9	4.04×10^7	2.30×10^3	4.06×10^4	5.60×10^{-1}	4.61×10^0	-2.52×10^{-1}
10	5.25×10^6	1.07×10^3	7.99×10^3	4.20×10^{-1}	3.90×10^0	-3.77×10^{-1}
11	5.25×10^6	1.07×10^3	7.99×10^3	5.60×10^{-1}	3.90×10^0	-2.52×10^{-1}
12	2.05×10^6	2.30×10^2	7.99×10^3	4.20×10^{-1}	3.90×10^0	-3.77×10^{-1}
13	2.05×10^6	2.30×10^2	7.99×10^3	5.60×10^{-1}	3.90×10^0	-2.52×10^{-1}
14	1.30×10^6	2.30×10^2	5.55×10^3	4.20×10^{-1}	3.74×10^0	-3.77×10^{-1}
15	1.30×10^6	2.30×10^2	5.55×10^3	5.60×10^{-1}	3.74×10^0	-2.52×10^{-1}
16	7.75×10^5	2.30×10^2	1.38×10^3	4.20×10^{-1}	3.14×10^0	-3.77×10^{-1}

3.3 Experiments with Raman spectra of minerals

We examine another seven experiments with Raman spectrum datafiles of minerals. The process is exactly the same as in section 3.2.

3.3.1 The Raman spectrum of datolite

The datafile of Raman spectrum of mineral datolite is the datafile through which we continue the experiments. This datafile contains 1024 pairs of data which are fed to L2WPMA with different values of k , k in $\{1, 2, \dots, 20\}$. The corresponding results are presented in Datolite.xlsx. Fig. 3.11 is the corresponding figure in which are shown the data and the best fit for $k = 14$.

In addition, for $k = 20$ the method detects 19 turning points, 10 of which are peaks. Table 3.3 presents the turning points positions by piecewise monotonic fits to the datolite data for values of k in $\{2, 4, \dots, 20\}$, so that we explore the behavior of the approximation. In the right part of Table 3.3 we indicate the positions of the turning points of each optimal fit for k in $\{2, 4, \dots, 20\}$ in correspondence with the column labeled “ t_j ”, derived when $k = 20$. For instance, when $k = 6$ the turning points occur at the positions 18, 103, 517, 618 and 909 as indicated by the times signs in the column labeled “6” and when $k = 8$ the method detects two more turning points at the positions 227 and 392 as indicated by the times signs in the column labeled “8”.

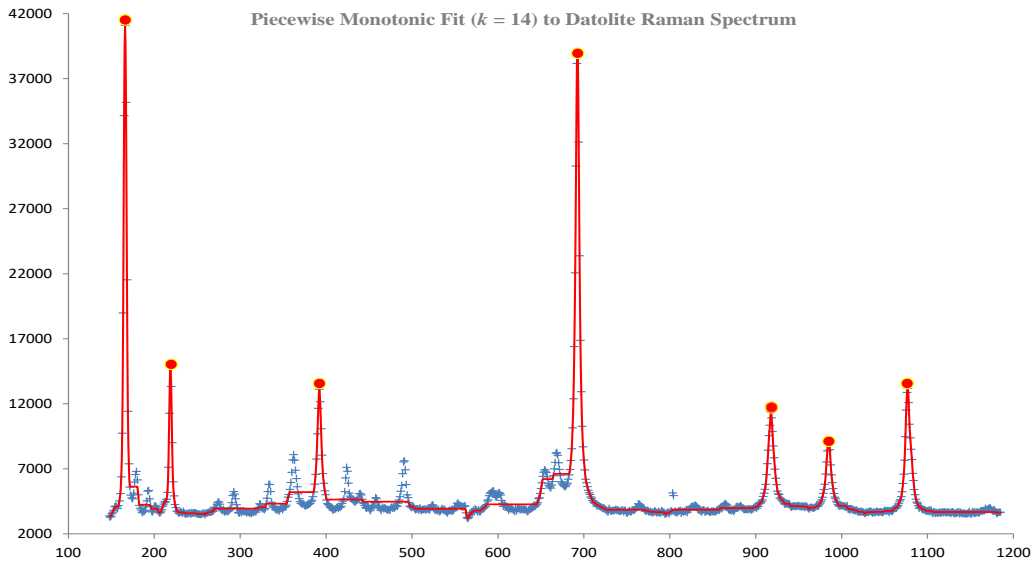


Figure 3.11: Detected peaks (circles) by a best monotonic fit with $k = 14$ to 1024 data points (plus signs) of the datolite Raman spectrum. The solid line illustrates the best fit. The numbers give the intensities at the corresponding Raman shifts.

Table 3.3: Left four columns: Turning points in the datolite spectrum by a best fit with $k = 20$ monotonic sections. Right ten columns: The turning point positions of the optimal fit for k in $\{2, 4, \dots, 20\}$ are indicated by the times sign

j	t_j	x_{t_j}	Intensity (ϕ_{t_j})	$k =$	2	4	6	8	10	12	14	16	18	20
0	1	1.48×10^2	3.38×10^3		×	×	×	×	×	×	×	×	×	×
1	18	1.66×10^2	4.11×10^4			×	×	×	×	×	×	×	×	×
2	55	2.07×10^2	3.61×10^3							×	×	×	×	×
3	66	2.19×10^2	1.48×10^4							×	×	×	×	×
4	103	2.59×10^2	3.47×10^3			×	×	×	×	×	×	×	×	×
5	199	3.62×10^2	8.10×10^3										×	×
6	212	3.76×10^2	4.14×10^3										×	×
7	227	3.92×10^2	1.31×10^4					×	×	×	×	×	×	×
8	242	4.08×10^2	3.81×10^3											×
9	257	4.24×10^2	7.12×10^3											×
10	304	4.73×10^2	3.81×10^3									×	×	×
11	321	4.91×10^2	7.62×10^3									×	×	×
12	392	5.65×10^2	3.18×10^3					×	×	×	×	×	×	×
13	517	6.93×10^2	3.89×10^4		×	×	×	×	×	×	×	×	×	×
14	618	7.94×10^2	3.52×10^3				×	×	×	×	×	×	×	×
15	743	9.17×10^2	1.14×10^4						×	×	×	×	×	×
16	789	9.62×10^2	3.91×10^3								×	×	×	×
17	812	9.84×10^2	9.04×10^3								×	×	×	×
18	857	1.03×10^3	3.57×10^3						×	×	×	×	×	×
19	909	1.08×10^3	1.32×10^4				×	×	×	×	×	×	×	×
20	1024	1.18×10^3	3.66×10^3		×	×	×	×	×	×	×	×	×	×

The value of centralized measures which are mentioned in section 3.1 when k in $\{1, 2, \dots, 20\}$ are presented in Table 3.4. The values of the measures decrease while the number of monotonic sections increases. More specifically, the order of magnitude of the sum of squares of residuals starts from 10^9 for k in $\{1, 2, \dots, 7\}$, decreases to 10^8 for k in $\{8, 9, \dots, 17\}$ and to 10^7 for k in $\{18, 19, 20\}$. For k in $\{2, 3, \dots, 19\}$ the values are equal per two. The order of magnitude of maximum absolute value of estimated errors is 10^4 and it reduces to 10^3 , 9.70×10^3 for k in $\{4, 5, \dots, 11\}$, 4.27×10^3 for k in $\{12, 13\}$, 3.15×10^3 for k in $\{14, 15\}$, 2.88×10^3 for k in $\{16, 17\}$, 2.48×10^3 for k in $\{18, 19\}$ and 1.63×10^3 for $k = 20$. The order of magnitude of the maximum absolute value of the Lagrange multipliers declines from 10^5 for k in $\{1, 2, \dots, 9\}$ to 10^4 for k in $\{10, 11, \dots, 20\}$. More specifically, for k in $\{6, 7, \dots, 17\}$ the values are equal per two, for k in $\{3, 4, 5\}$ and $\{18, 19, 20\}$ are equal per three and for k in $\{1, 2\}$ are different. The minimum absolute value of nonzero Lagrange multipliers is 1.10×10^1 for k in $\{1, 2\}$, 2.00×10^0 for k in $\{3, 4, \dots, 9\}$ and 1.00×10^0 for k in $\{10, 11, \dots, 20\}$. Their decadic logarithms display a corresponding behavior.

Table 3.4: Measures for Datolite

k	SSR	D	L	ℓ	$\log_{10}L$	$\log_{10}\ell$
1	9.51×10^9	3.39×10^4	5.39×10^5	1.10×10^1	5.73×10^0	1.04×10^0
2	5.41×10^9	3.63×10^4	3.31×10^5	1.10×10^1	5.52×10^0	1.04×10^0
3	4.49×10^9	3.02×10^4	2.13×10^5	2.00×10^0	5.33×10^0	3.01×10^{-1}
4	1.61×10^9	9.70×10^3	2.13×10^5	2.00×10^0	5.33×10^0	3.01×10^{-1}
5	1.61×10^9	9.70×10^3	2.13×10^5	2.00×10^0	5.33×10^0	3.01×10^{-1}
6	1.15×10^9	9.70×10^3	1.45×10^5	2.00×10^0	5.16×10^0	3.01×10^{-1}
7	1.15×10^9	9.70×10^3	1.45×10^5	2.00×10^0	5.16×10^0	3.01×10^{-1}
8	8.15×10^8	9.70×10^3	1.23×10^5	2.00×10^0	5.09×10^0	3.01×10^{-1}
9	8.15×10^8	9.70×10^3	1.23×10^5	2.00×10^0	5.09×10^0	3.01×10^{-1}
10	5.28×10^8	9.70×10^3	6.17×10^4	1.00×10^0	4.79×10^0	0.00×10^0
11	5.28×10^8	9.70×10^3	6.17×10^4	1.00×10^0	4.79×10^0	0.00×10^0
12	2.76×10^8	4.27×10^3	5.80×10^4	1.00×10^0	4.76×10^0	0.00×10^0
13	2.76×10^8	4.27×10^3	5.80×10^4	1.00×10^0	4.76×10^0	0.00×10^0
14	1.71×10^8	3.15×10^3	3.11×10^4	1.00×10^0	4.49×10^0	0.00×10^0
15	1.71×10^8	3.15×10^3	3.11×10^4	1.00×10^0	4.49×10^0	0.00×10^0
16	1.29×10^8	2.88×10^3	2.69×10^4	1.00×10^0	4.43×10^0	0.00×10^0
17	1.29×10^8	2.88×10^3	2.69×10^4	1.00×10^0	4.43×10^0	0.00×10^0
18	9.03×10^7	2.48×10^3	2.46×10^4	1.00×10^0	4.39×10^0	0.00×10^0
19	9.03×10^7	2.48×10^3	2.46×10^4	1.00×10^0	4.39×10^0	0.00×10^0
20	6.81×10^7	1.63×10^3	2.46×10^4	1.00×10^0	4.39×10^0	0.00×10^0

3.3.2 The Raman spectrum of olivenite

We continue the experiments with the Raman spectrum datafile of the mineral olivenite in which the number of pairs of data is 1024. We feed the data to L2WPMA with k in $\{1, 2, \dots, 16\}$ and the results are presented in Olivenite.xlsx with the corresponding measures which we calculate. The main features of this data set may easily be captured by Fig. 3.12 which shows the data and the best fit for $k = 14$.

Furthermore, for $k = 16$ the method detects 15 turning points, 8 of which are peaks. In order to examine the behavior of the approximation, we display the turning points by piecewise monotonic fits to the olivenite data for values of k in $\{2, 4, \dots, 16\}$ in Table 3.5. In the right part of the table 3.5 are indicated the positions of the turning points of each optimal fit for k in $\{2, 4, \dots, 16\}$ in correspondence with the column labeled “ t_j ”, derived when $k = 16$. For example, for $k = 6$ the turning points occur at the positions 66, 99, 121, 527 and 710 as shown by the times signs in the column labeled “6”, while for $k = 8$ two more turning points occur at the positions 158 and 177 as indicated by the times signs in the column labeled “8”.

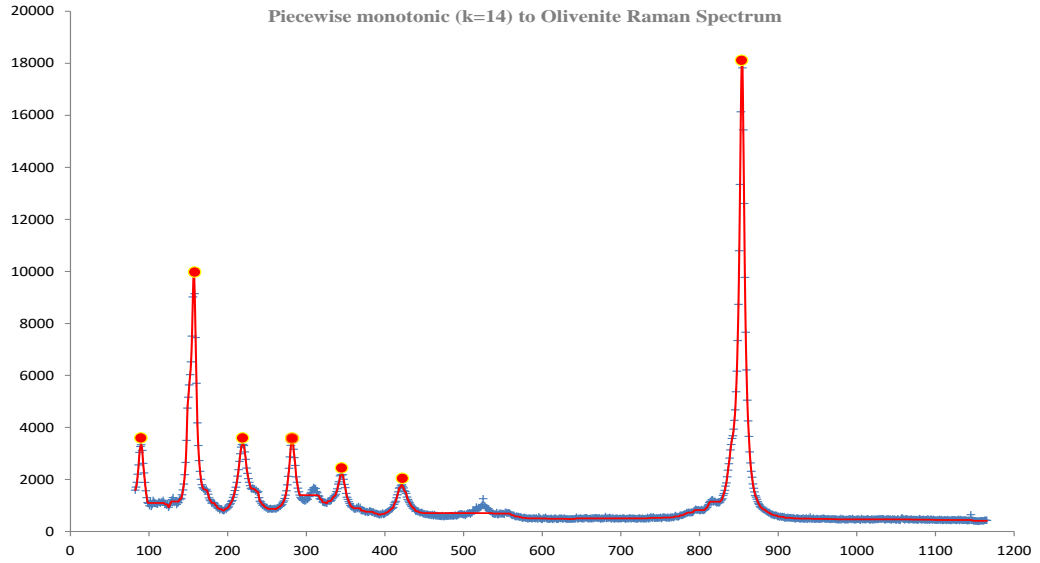


Figure 3.12: Detected peaks (circles) by a best monotonic fit with $k = 14$ to 1024 data points (plus signs) of the olivinite Raman spectrum. The solid line illustrates the best fit. The numbers give the intensities at the corresponding Raman shifts.

Table 3.5: Left four columns: Turning points in the olivinite spectrum by a best fit with $k = 16$ monotonic sections. Right eight columns: The turning point positions of the optimal fit for k in $\{2, 4, \dots, 16\}$ are indicated by the times sign

j	t_j	x_{t_j}	Intensity (ϕ_{t_j})	$k =$	2	4	6	8	10	12	14	16
0	1	8.25×10^1	1.60×10^3		×	×	×	×	×	×	×	×
1	8	9.02×10^1	3.34×10^3						×	×	×	×
2	38	1.25×10^2	9.32×10^2						×	×	×	×
3	66	1.57×10^2	9.95×10^3			×	×	×	×	×	×	×
4	99	1.94×10^2	8.06×10^2				×	×	×	×	×	×
5	121	2.19×10^2	3.35×10^3				×	×	×	×	×	×
6	158	2.61×10^2	8.57×10^2					×	×	×	×	×
7	177	2.83×10^2	3.46×10^3					×	×	×	×	×
8	216	3.26×10^2	1.09×10^3								×	×
9	233	3.45×10^2	2.19×10^3								×	×
10	276	3.93×10^2	6.43×10^2							×	×	×
11	302	4.21×10^2	1.79×10^3							×	×	×
12	352	4.76×10^2	5.79×10^2									×
13	397	5.25×10^2	1.26×10^3									×
14	527	6.33×10^2	4.71×10^2			×	×	×	×	×	×	×
15	710	8.54×10^2	1.80×10^4		×	×	×	×	×	×	×	×
16	1024	1.17×10^3	4.32×10^2		×	×	×	×	×	×	×	×

Table 3.6 presents the measures which we examine for each k in $\{1, 2, \dots, 16\}$. It is observed that the values of the sum of squares of errors decreases while the number of monotonic sections k increases. More specifically, its order of magnitude starts from 10^9 for $k = 1$, decreases to 10^8 for k in $\{2, 3\}$ and to 10^7 for k in $\{4, 5, \dots, 11\}$. Then it decreases to 10^6 for k in $\{12, 13, 14, 15\}$ and to 10^5 for $k = 16$. The order of magnitude of maximum absolute values of estimated errors decreases gradually for k in $\{1, 2, 3\}$,

from 1.69×10^4 to 7.53×10^3 . For k in $\{4, 5, 6, 7\}$ the value is 1.99×10^3 and for $k = 8$ is 1.90×10^3 . Then it presents a fluctuation while k increases, that is for k in $\{9, 11, 13\}$ the value is 9.42×10^2 and for $k = 10$ and $k = 12$ the values are 8.24×10^2 and 7.48×10^2 respectively. The value for $k = 14$ and $k = 15$ is 5.52×10^2 and for $k = 16$ is 2.94×10^2 . The order of magnitude of the maximum absolute value of nonzero Lagrange multipliers for k in $\{1, 2, 3\}$ is 10^5 . Then its order of magnitude for k in $\{4, 5, \dots, 12\}$ decreases to 10^3 . Its values are equal per two except for $k = 8$. For k in $\{13, 14, 15\}$ its value is 8.72×10^3 and for $k = 16$ is 3.23×10^3 . The minimum absolute value of nonzero Lagrange multipliers for k in $\{1, 2\}$ is equal to 1.00×10^0 and for k in $\{3, 4, \dots, 16\}$ is equal to 5.33×10^{-1} . Their decadic logarithms have a corresponding behavior.

Table 3.6: Measures for Olivenite

k	SSR	D	L	ℓ	$\log_{10}L$	$\log_{10}\ell$
1	2.27×10^9	1.69×10^4	3.71×10^5	1.00×10^0	5.57×10^0	0.00×10^0
2	6.62×10^8	8.87×10^3	3.44×10^5	1.00×10^0	5.54×10^0	0.00×10^0
3	4.13×10^8	7.53×10^3	1.09×10^5	5.33×10^{-1}	5.04×10^0	-2.73×10^{-1}
4	9.52×10^7	1.99×10^3	3.32×10^4	5.33×10^{-1}	4.52×10^0	-2.73×10^{-1}
5	7.80×10^7	1.99×10^3	3.32×10^4	5.33×10^{-1}	4.52×10^0	-2.73×10^{-1}
6	6.38×10^7	1.99×10^3	2.94×10^4	5.33×10^{-1}	4.47×10^0	-2.73×10^{-1}
7	4.67×10^7	1.99×10^3	2.94×10^4	5.33×10^{-1}	4.47×10^0	-2.73×10^{-1}
8	3.51×10^7	1.90×10^3	2.48×10^4	5.33×10^{-1}	4.40×10^0	-2.73×10^{-1}
9	1.79×10^7	9.42×10^2	1.79×10^4	5.33×10^{-1}	4.25×10^0	-2.73×10^{-1}
10	1.41×10^7	8.24×10^2	1.79×10^4	5.33×10^{-1}	4.25×10^0	-2.73×10^{-1}
11	1.06×10^7	9.42×10^2	1.06×10^4	5.33×10^{-1}	4.02×10^0	-2.73×10^{-1}
12	6.76×10^6	7.48×10^2	1.06×10^4	5.33×10^{-1}	4.02×10^0	-2.73×10^{-1}
13	6.35×10^6	9.42×10^2	8.72×10^3	5.33×10^{-1}	3.94×10^0	-2.73×10^{-1}
14	2.48×10^6	5.52×10^2	8.72×10^3	5.33×10^{-1}	3.94×10^0	-2.73×10^{-1}
15	2.48×10^6	5.52×10^2	8.72×10^3	5.33×10^{-1}	3.94×10^0	-2.73×10^{-1}
16	9.83×10^5	2.94×10^2	3.23×10^3	5.33×10^{-1}	3.51×10^0	-2.73×10^{-1}

3.3.3 The Raman spectrum of clintonite

The next datafile which we deal with is a Raman spectrum of mineral clintonite. The number of pairs of data is 1024. We test it for k in $\{1, 2, \dots, 14\}$. For each value of $\{1, 2, \dots, 14\}$ we feed the data to L2WPMA and the corresponding results are presented in fourteen different sheets, one sheet for each k , in Clintonite.xlsx. In order to capture the main features of the data set, we present Fig. 3.13 for $k = 12$.

Moreover, for $k = 14$ the method detects 13 turning points, 6 of which are peaks. In Table 3.7 are presented the turning point positions by piecewise monotonic fits to the clintonite data for values of k in $\{2, 4, \dots, 14\}$ in order to investigate the behavior of the

approximation. In the right part of Table 3.7 we indicate the positions of the turning points of each optimal fit for k in $\{2, 4, \dots, 14\}$ in correspondence with the column labeled “ t_j ”, derived when $k = 14$. For example, when $k = 6$ the turning points occur at the positions 125, 165, 511, 587 and 989 as indicated by the times signs in the column labeled “6”.

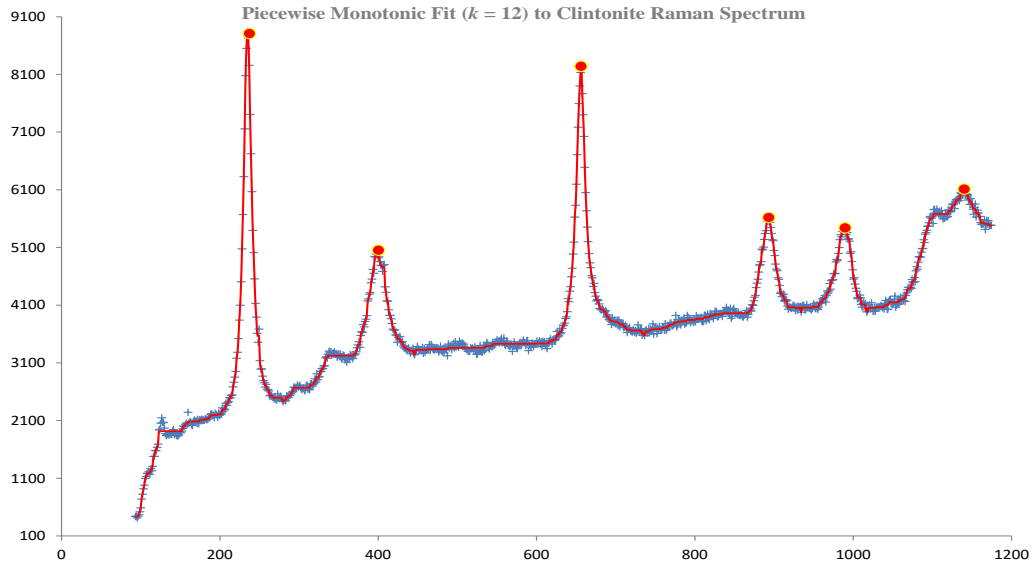


Figure 3.13: Detected peaks (circles) by a best monotonic fit with $k = 12$ to 1024 data points (plus signs) of the clintonite Raman spectrum. The solid line illustrates the best fit. The numbers give the intensities at the corresponding Raman shifts.

Table 3.7: Left four columns: Turning points in the clintonite spectrum by a best fit with $k = 14$ monotonic sections. Right seven columns: The turning point positions of the optimal fit for k in $\{2, 4, \dots, 14\}$ are indicated by the times sign

j	t_j	x_{t_j}	Intensity (ϕ_{t_j})	$k =$	2	4	6	8	10	12	14
0	1	9.34×10^1	4.39×10^2		×	×	×	×	×	×	×
1	30	1.26×10^2	2.15×10^3								×
2	47	1.46×10^2	1.84×10^3								×
3	125	2.35×10^2	8.85×10^3			×	×	×	×	×	×
4	165	2.80×10^2	2.43×10^3			×	×	×	×	×	×
5	272	3.99×10^2	5.00×10^3					×	×	×	×
6	315	4.46×10^2	3.24×10^3					×	×	×	×
7	511	6.57×10^2	8.21×10^3				×	×	×	×	×
8	587	7.36×10^2	3.57×10^3				×	×	×	×	×
9	739	8.93×10^2	5.60×10^3						×	×	×
10	780	9.34×10^2	3.98×10^3						×	×	×
11	834	9.88×10^2	5.46×10^3							×	×
12	863	1.02×10^3	3.98×10^3							×	×
13	989	1.14×10^3	6.07×10^3		×	×	×	×	×	×	×
14	1024	1.17×10^3	5.48×10^3		×	×	×	×	×	×	×

The centralized measures which we examine and calculate from the above results are presented in Table 3.8. It is observed that the value of measures decrease while the number of monotonic sections increases. More specifically, the order of magnitude of the sum of

squares of residuals starts from 10^9 for $k = 1$, then decreases to 10^8 for k in $\{2, 3, 4, 5\}$ and to 10^7 for k in $\{6, 7, \dots, 11\}$. For k in $\{12, 13, 14\}$ it falls to 10^6 . Except for $k = 1$ and $k = 14$ the values are equal per two. A reduction is noted in the maximum absolute values of the estimated error. The order of magnitude is 10^3 for k in $\{1, 2, \dots, 11\}$ and falls to 10^2 for k in $\{12, 13, 14\}$. The same condition as above is detected. The order of magnitude of maximum absolute value of nonzero Lagrange multipliers is 10^5 for k in $\{1, 2, \dots, 5\}$ and decreases to 10^4 for k in $\{6, 7, \dots, 11\}$. In the latter case the values are equal per two. For k in $\{12, 13, 14\}$ the values are equal to 1.68×10^3 . The minimum absolute value of nonzero Lagrange multipliers is 3.29×10^3 for $k = 1$, decreases to 8.00×10^{-1} for k in $\{2, 3, \dots, 7\}$ and to 5.00×10^{-1} for k in $\{8, 9, \dots, 14\}$. Their decadic logarithms have the same behavior respectively.

Table 3.8: Measures for Clintonite

k	SSR	D	L	ℓ	$\log_{10}L$	$\log_{10}\ell$
1	1.41×10^9	5.01×10^3	7.11×10^5	3.29×10^3	5.85×10^0	3.52×10^0
2	4.81×10^8	5.48×10^3	1.12×10^5	8.00×10^{-1}	5.09×10^0	-9.70×10^{-2}
3	4.81×10^8	5.48×10^3	1.12×10^5	8.00×10^{-1}	5.09×10^0	-9.70×10^{-2}
4	2.34×10^8	4.09×10^3	1.06×10^5	8.00×10^{-1}	5.02×10^0	-9.70×10^{-2}
5	2.34×10^8	4.09×10^3	1.06×10^5	8.00×10^{-1}	5.02×10^0	-9.70×10^{-2}
6	7.78×10^7	1.45×10^3	5.90×10^4	8.00×10^{-1}	4.77×10^0	-9.70×10^{-2}
7	7.78×10^7	1.45×10^3	5.90×10^4	8.00×10^{-1}	4.77×10^0	-9.70×10^{-2}
8	4.18×10^7	1.19×10^3	3.69×10^4	5.00×10^{-1}	4.57×10^0	-3.01×10^{-1}
9	4.18×10^7	1.19×10^3	3.69×10^4	5.00×10^{-1}	4.57×10^0	-3.01×10^{-1}
10	2.06×10^7	1.05×10^3	3.64×10^4	5.00×10^{-1}	4.56×10^0	-3.01×10^{-1}
11	2.06×10^7	1.05×10^3	3.64×10^4	5.00×10^{-1}	4.56×10^0	-3.01×10^{-1}
12	1.23×10^6	2.33×10^2	1.68×10^3	5.00×10^{-1}	3.22×10^0	-3.01×10^{-1}
13	1.23×10^6	2.33×10^2	1.68×10^3	5.00×10^{-1}	3.22×10^0	-3.01×10^{-1}
14	1.06×10^6	1.63×10^2	1.68×10^3	5.00×10^{-1}	3.22×10^0	-3.01×10^{-1}

3.3.4 The Raman spectrum of beryl

In the next experiment we use the datafile of Raman spectrum of mineral beryl. It consists of 1000 pairs of data and is tested for k in $\{1, 2, \dots, 14\}$. Feeding the data to L2WPMA, the results are presented in fourteen different sheets, in Beryl.xlsx, with the corresponding calculations of measures which are studied. Fig. 3.14 displays the data and the best fit for $k = 14$, so as to capture the main features.

Moreover, for $k = 14$ the method detects 13 turning points, 7 of which are peaks. The behavior of the approximation is explored by presenting in Table 3.9 the turning point positions by piecewise monotonic fits to the beryl data for values of k in $\{2, 4, \dots, 14\}$. In

the right part of Table 3.9 we indicate the positions of the turning points of each optimal fit for k in $\{2, 4, \dots, 14\}$ in correspondence with the column labeled “ t_j ”, derived when $k = 14$. For example, when $k = 4$ the turning points occur at the positions 534, 681 and 926 as displayed by the times signs in the column labeled “4”.

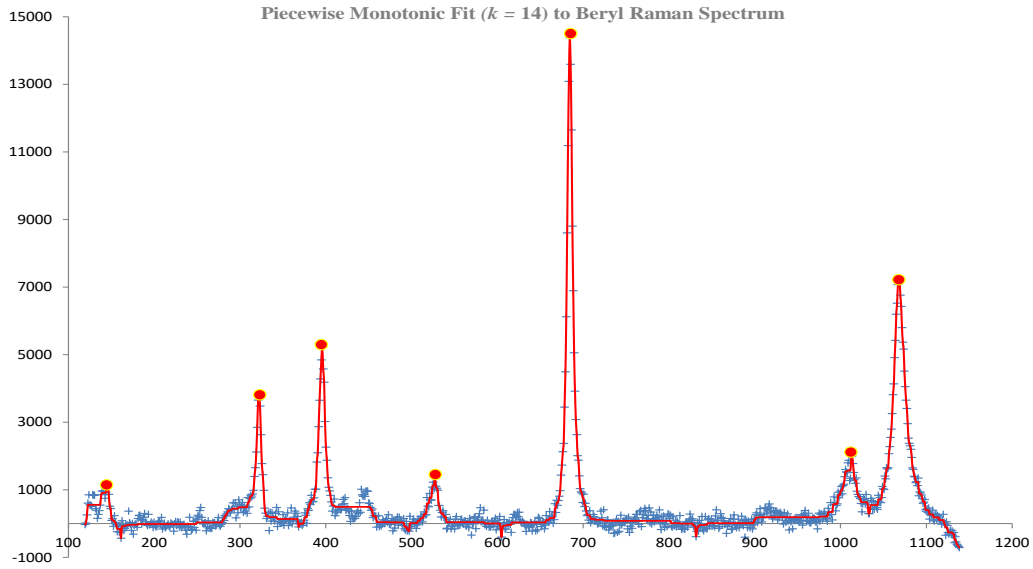


Figure 3.14: Detected peaks (circles) by a best monotonic fit with textitk = 14 to 1000 data points (plus signs) of the beryl Raman spectrum. The solid line illustrates the best fit. The numbers give the intensities at the corresponding Raman shifts.

Table 3.9: Left four columns: Turning points in the beryl spectrum by a best fit with $k = 14$ monotonic sections. Right seven columns: The turning point positions of the optimal fit for k in $\{2, 4, \dots, 14\}$ are indicated by the times sign

j	t_j	x_{t_j}	Intensity (ϕ_{t_j})	$k =$	2	4	6	8	10	12	14
0	1	1.19×10^2	-2.81×10^1		×	×	×	×	×	×	×
1	25	1.46×10^2	1.14×10^3						×	×	×
2	39	1.61×10^2	-4.33×10^2						×	×	×
3	187	3.22×10^2	3.76×10^3					×	×	×	×
4	230	3.68×10^2	-9.95×10^1					×	×	×	×
5	256	3.96×10^2	5.21×10^3				×	×	×	×	×
6	352	4.97×10^2	-2.22×10^2								×
7	381	5.27×10^2	1.39×10^3								×
8	456	6.05×10^2	-3.98×10^2				×	×	×	×	×
9	534	6.84×10^2	1.44×10^4		×	×	×	×	×	×	×
10	681	8.32×10^2	-3.87×10^2			×	×	×	×	×	×
11	868	1.01×10^3	2.00×10^3							×	×
12	889	1.03×10^3	4.62×10^2							×	×
13	926	1.07×10^3	7.19×10^3			×	×	×	×	×	×
14	1000	1.14×10^3	-7.11×10^2		×	×	×	×	×	×	×

In Table 3.10 we present the value of centralized measures which are studied as k increases, k in $\{1, 2, \dots, 14\}$. While the number of monotonic sections increases the order of magnitude of the sum of squares of residuals goes down. For $k = 1$ is 10^9 , for

k in $\{2, 3, \dots, 6\}$ is 10^8 and for k in $\{7, 8, \dots, 14\}$ is 10^7 . Respectively, a decrease is observed in absolute values of estimated errors. More specifically, the corresponding order of magnitude is 10^4 for $k = 1$, 10^3 for k in $\{2, 3, \dots, 7\}$, equal per two, and for k in $\{8, 9, \dots, 12\}$, all equal, and 10^2 for k in $\{13, 14\}$. The maximum absolute value of nonzero Lagrange multipliers is 2.88×10^5 , 2.83×10^5 for k in $\{2, 3\}$ and 1.19×10^5 for k in $\{4, 5\}$. It drops to 4.16×10^4 for k in $\{6, 7\}$, 2.92×10^4 for $k = 8$ and 2.06×10^4 for k in $\{9, 10, 11, 12\}$. For k in $\{13, 14\}$ is 7.49×10^3 . The minimum absolute value of the nonzero Lagrange multipliers is equal to 2.84×10^0 for all values of k . The behavior of their decadic logarithms follows the same pattern.

Table 3.10: Measures for Beryl

k	SSR	D	L	ℓ	$\log_{10}L$	$\log_{10}\ell$
1	1.91×10^9	1.38×10^4	2.88×10^5	2.84×10^0	5.46×10^0	4.54×10^{-1}
2	8.32×10^8	6.62×10^3	2.83×10^5	2.84×10^0	5.45×10^0	4.54×10^{-1}
3	8.22×10^8	6.62×10^3	2.83×10^5	2.84×10^0	5.45×10^0	4.54×10^{-1}
4	2.52×10^8	4.82×10^3	1.19×10^5	2.84×10^0	5.08×10^0	4.54×10^{-1}
5	2.42×10^8	4.82×10^3	1.19×10^5	2.84×10^0	5.08×10^0	4.54×10^{-1}
6	1.02×10^8	3.18×10^3	4.16×10^4	2.84×10^0	4.62×10^0	4.54×10^{-1}
7	9.26×10^7	3.18×10^3	4.16×10^4	2.84×10^0	4.62×10^0	4.54×10^{-1}
8	4.87×10^7	1.17×10^3	2.92×10^4	2.84×10^0	4.47×10^0	4.54×10^{-1}
9	3.91×10^7	1.17×10^3	2.06×10^4	2.84×10^0	4.31×10^0	4.54×10^{-1}
10	3.71×10^7	1.17×10^3	2.06×10^4	2.84×10^0	4.31×10^0	4.54×10^{-1}
11	2.88×10^7	1.17×10^3	2.06×10^4	2.84×10^0	4.31×10^0	4.54×10^{-1}
12	2.68×10^7	1.17×10^3	2.06×10^4	2.84×10^0	4.31×10^0	4.54×10^{-1}
13	1.92×10^7	6.65×10^2	7.49×10^3	2.84×10^0	3.87×10^0	4.54×10^{-1}
14	1.71×10^7	5.21×10^2	7.49×10^3	2.84×10^0	3.87×10^0	4.54×10^{-1}

3.3.5 The Raman spectrum of lizardite

Continuing the experiments, we use the Raman spectrum datafile of mineral lizardite which consists of 1008 pairs of data. For each value of k in $\{1, 2, \dots, 14\}$ we feed the data to L2WPMA. The corresponding results are presented in fourteen sheets, one for each k , in Lizardite.xlsx. The data and the best fit for $k = 14$ are displayed in Fig. 3.15, with the aim of detecting the main features of the data.

Furthermore, for $k = 14$ the method detects 13 turning points, 7 of which are peaks. Table 3.11 presents the turning point positions by piecewise monotonic fits to the lizardite data for values of k in $\{2, 4, \dots, 14\}$, so that we explore the behavior of the approximation. In the right part of Table 3.11 we indicate the positions of the turning points of each optimal fit for k in $\{2, 4, \dots, 14\}$ in correspondence with the column labeled “ t_j ”, derived when

$k = 14$. For instance, when $k = 8$ the turning points occur at the positions 18, 59, 102, 129, 240, 288 and 523 as indicated by the times signs in the column labeled “8”.

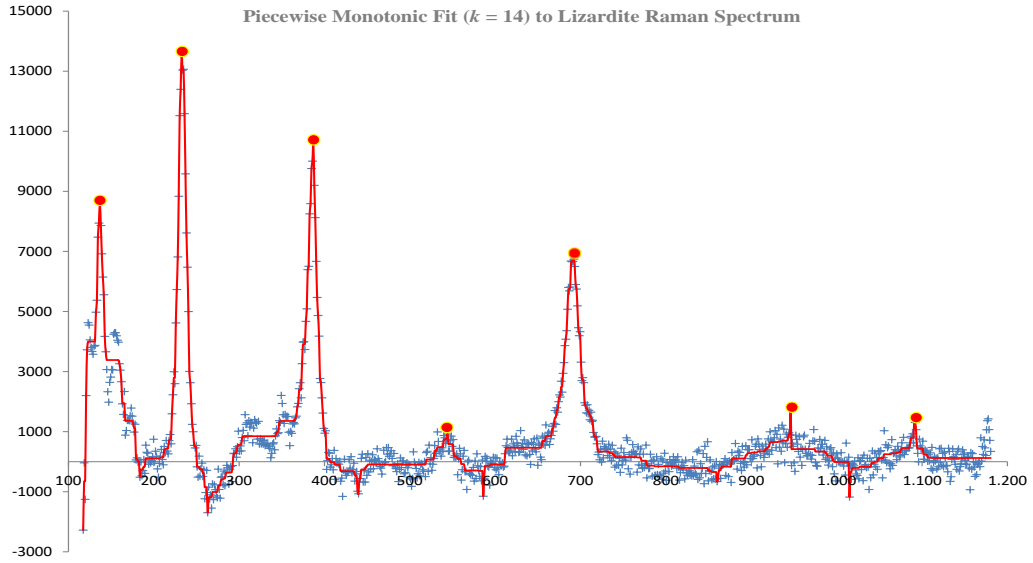


Figure 3.15: Detected peaks (circles) by a best monotonic fit with $k = 14$ to 1008 data points (plus signs) of the lizardite Raman spectrum. The solid line illustrates the best fit. The numbers give the intensities at the corresponding Raman shifts.

Table 3.11: Left four columns: Turning points in the lizardite spectrum by a best fit with $k = 14$ monotonic sections. Right seven columns: The turning point positions of the optimal fit for k in $\{2, 4, \dots, 14\}$ are indicated by the times sign

j	t_j	x_{t_j}	Intensity (ϕ_{t_j})	$k =$	2	4	6	8	10	12	14
0	1	1.17×10^2	-2.28×10^3		×	×	×	×	×	×	×
1	18	1.37×10^2	8.58×10^3					×	×	×	×
2	59	1.84×10^2	-5.19×10^2					×	×	×	×
3	102	2.33×10^2	1.35×10^4		×	×	×	×	×	×	×
4	129	2.63×10^2	-1.70×10^3			×	×	×	×	×	×
5	240	3.87×10^2	1.06×10^4			×	×	×	×	×	×
6	288	4.40×10^2	-1.07×10^3				×	×	×	×	×
7	384	5.44×10^2	9.18×10^2								×
8	423	5.87×10^2	-5.53×10^2								×
9	523	6.92×10^2	6.74×10^3				×	×	×	×	×
10	685	8.60×10^2	-6.65×10^2						×	×	×
11	770	9.46×10^2	1.73×10^3						×	×	×
12	839	1.02×10^3	-1.18×10^3							×	×
13	916	1.09×10^3	1.46×10^3							×	×
14	1008	1.18×10^3	3.40×10^2		×	×	×	×	×	×	×

The measures which we study derive from the calculations of the above results and are presented in Table 3.12. While the value of k increases the order of magnitude of the sum of squares of residuals decreases gradually. For k in $\{1, 2, 3, 4\}$ is 10^9 , for k in $\{5, 6, \dots, 11\}$ decreases to 10^8 and for k in $\{12, 13, 14\}$ to 10^7 . For k in $\{8, 9, \dots, 13\}$ the values are equal per two. The maximum absolute value of estimated errors starts from 1.11×10^4

for $k = 1$ and reduces to 9.27×10^3 for $k = 2$ and $k = 3$. For k in $\{4, 5, 6, 7\}$ the values are 6.49×10^3 and 6.60×10^3 alternately. Then it decreases to 1.60×10^3 for $k = 8$ and $k = 9$ and 1.40×10^3 for k in $\{10, 11, \dots, 14\}$. The maximum absolute value of nonzero Lagrange multipliers decreases from 2.60×10^5 for k in $\{1, 2, \dots, 5\}$, to 1.64×10^5 for k in $\{6, 7, 8\}$ and to 2.97×10^4 . Then it decreases to 2.42×10^4 and to 1.46×10^4 . The absolute value of the nonzero Lagrange multipliers is 9.44×10^{-1} in all cases. Their decadic logarithms have the same behavior respectively.

Table 3.12: Measures for Lizardite

k	SSR	D	L	ℓ	$\log_{10}L$	$\log_{10}\ell$
1	2.69×10^9	1.11×10^4	2.60×10^5	9.44×10^{-1}	5.42×10^0	-2.49×10^{-2}
2	1.94×10^9	9.27×10^3	2.60×10^5	9.44×10^{-1}	5.42×10^0	-2.49×10^{-2}
3	1.68×10^9	9.27×10^3	2.60×10^5	9.44×10^{-1}	5.42×10^0	-2.49×10^{-2}
4	1.15×10^9	6.49×10^3	2.60×10^5	9.44×10^{-1}	5.42×10^0	-2.49×10^{-2}
5	8.91×10^8	6.60×10^3	2.60×10^5	9.44×10^{-1}	5.42×10^0	-2.49×10^{-2}
6	5.54×10^8	6.49×10^3	1.64×10^5	9.44×10^{-1}	5.21×10^0	-2.49×10^{-2}
7	2.96×10^8	6.60×10^3	6.79×10^4	9.44×10^{-1}	4.83×10^0	-2.49×10^{-2}
8	1.31×10^8	1.60×10^3	6.79×10^4	9.44×10^{-1}	4.83×10^0	-2.49×10^{-2}
9	1.31×10^8	1.60×10^3	6.79×10^4	9.44×10^{-1}	4.83×10^0	-2.49×10^{-2}
10	1.04×10^8	1.40×10^3	2.97×10^4	9.44×10^{-1}	4.47×10^0	-2.49×10^{-2}
11	1.04×10^8	1.40×10^3	2.97×10^4	9.44×10^{-1}	4.47×10^0	-2.49×10^{-2}
12	9.10×10^7	1.40×10^3	2.42×10^4	9.44×10^{-1}	4.38×10^0	-2.49×10^{-2}
13	9.10×10^7	1.40×10^3	2.42×10^4	9.44×10^{-1}	4.38×10^0	-2.49×10^{-2}
14	8.02×10^7	1.40×10^3	1.46×10^4	9.44×10^{-1}	4.17×10^0	-2.49×10^{-2}

3.3.6 The Raman spectrum of hemimorphite

The next experiment with Raman spectrum datafiles of minerals which we use is the datafile of hemimorphite. This datafile contains 1025 pairs of data. The data are fed to L2WPMA with k in $\{1, 2, \dots, 18\}$ and we obtain the results which are presented in Hemimorphite.xlsx, one sheet for each k . Fig. 3.16 shows the corresponding data and the best fit for $k = 16$.

In addition, for $k = 18$ the method detects 17 turning points, 9 of which are peaks. In Table 3.13 are presented the turning point positions by piecewise monotonic fits to the hemimorphite data for values of k in $\{2, 4, \dots, 18\}$ in order to investigate the behavior of the approximation. In the right part of Table 3.13 are indicated the positions of the turning points of each optimal fit for k in $\{2, 4, \dots, 18\}$ in correspondence with the column labeled “ t_j ”, derived when $k = 18$. For example, when $k = 6$ the turning points occur at the positions 20, 33, 52, 693 and 787 as indicated by the times signs in the column labeled “6”.

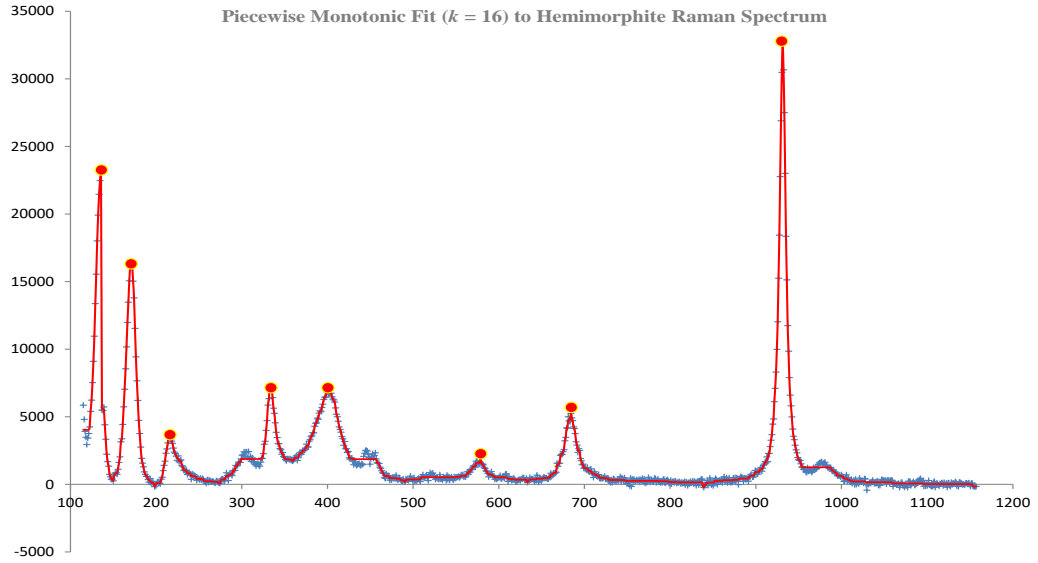


Figure 3.16: Detected peaks (circles) by a best monotonic fit with $k = 16$ to 1024 data points (plus signs) of the hemimorphite Raman spectrum. The solid line illustrates the best fit. The numbers give the intensities at the corresponding Raman shifts.

Table 3.13: Left four columns: Turning points in the hemimorphite spectrum by a best fit with $k = 18$ monotonic sections. Right nine columns: The turning point positions of the optimal fit for k in $\{2, 4, \dots, 18\}$ are indicated by the times sign

j	t_j	x_{t_j}	Intensity (ϕ_{t_j})	$k =$	2	4	6	8	10	12	14	16	18
0	1	1.15×10^2	5.86×10^3		×	×	×	×	×	×	×	×	×
1	1	1.15×10^2	5.86×10^3										×
2	5	1.19×10^2	2.94×10^3										×
3	20	1.36×10^2	2.32×10^4			×	×	×	×	×	×	×	×
4	33	1.50×10^2	2.53×10^2				×	×	×	×	×	×	×
5	52	1.71×10^2	1.63×10^4				×	×	×	×	×	×	×
6	77	1.98×10^2	-1.81×10^2								×	×	×
7	92	2.15×10^2	3.50×10^3								×	×	×
8	146	2.74×10^2	7.60×10^1					×	×	×	×	×	×
9	202	3.34×10^2	7.34×10^3							×	×	×	×
10	226	3.60×10^2	1.72×10^3							×	×	×	×
11	267	4.03×10^2	7.08×10^3					×	×	×	×	×	×
12	350	4.91×10^2	1.71×10^2									×	×
13	435	5.79×10^2	1.93×10^3									×	×
14	488	6.33×10^2	1.41×10^2						×	×	×	×	×
15	538	6.84×10^2	5.24×10^3						×	×	×	×	×
16	693	8.39×10^2	-2.32×10^2			×	×	×	×	×	×	×	×
17	787	9.31×10^2	3.25×10^4		×	×	×	×	×	×	×	×	×
18	1024	1.16×10^3	-1.58×10^2		×	×	×	×	×	×	×	×	×

In Table 3.14 are presented the centralized measures which we examine and calculate from the above results. It is observed that the sum of squares of residuals decreases while the number of monotonic sections k increases. Its order of magnitude starts from 10^9 for k in $\{1, 2, \dots, 7\}$, decreases to 10^8 for k in $\{8, 9, 10, 11\}$ and to 10^7 for k in $\{12, 13, \dots, 18\}$. The maximum absolute value of estimated errors falls as k increases. Its order of magnitude

is 10^4 for k in $\{1, 2, \dots, 5\}$. Then it falls to 10^3 for k in $\{6, 7, \dots, 16\}$ and to 1.83×10^3 and 1.29×10^3 for k in $\{14, 15, 16\}$ alternately. More specifically, for k in $\{6, 7, \dots, 13\}$ the values are equal per two. Then it decreases to 6.61×10^2 for $k = 15$ and $k = 16$. The maximum absolute value of nonzero Lagrange multipliers starts from 6.93×10^5 for $k = 1$, increases to 9.48×10^5 for $k = 2$ and decreases to 3.11×10^5 for k in $\{3, 4, \dots, 7\}$. For k in $\{8, 9, \dots, 15\}$ the values decrease and are equal per two. For k in $\{16, 17, 18\}$ the values are equal to 8.38×10^3 . The minimum absolute value of nonzero Lagrange multipliers starts from 1.07×10^1 for $k = 1$ and falls to 8.44×10^0 for $k = 2$. Then it falls more to 4.43×10^0 for k in $\{3, 4, \dots, 7\}$ and to 8.75×10^{-1} for k in $\{8, 9, \dots, 18\}$. Their decadic logarithms display a corresponding behavior.

Table 3.14: Measures for Hemimorphite

k	SSR	D	L	ℓ	$\log_{10}L$	$\log_{10}\ell$
1	9.98×10^9	3.11×10^4	6.93×10^5	1.07×10^1	5.84×10^0	1.03×10^0
2	6.00×10^9	2.15×10^4	9.48×10^5	8.44×10^0	5.98×10^0	9.26×10^{-1}
3	3.17×10^9	1.29×10^4	3.11×10^5	4.43×10^0	5.49×10^0	6.46×10^{-1}
4	2.18×10^9	1.03×10^4	3.11×10^5	4.43×10^0	5.49×10^0	6.46×10^{-1}
5	2.07×10^9	1.29×10^4	3.11×10^5	4.43×10^0	5.49×10^0	6.46×10^{-1}
6	1.08×10^9	5.08×10^3	3.11×10^5	4.43×10^0	5.49×10^0	6.46×10^{-1}
7	1.07×10^9	5.08×10^3	3.11×10^5	4.43×10^0	5.49×10^0	6.46×10^{-1}
8	4.35×10^8	4.32×10^3	1.35×10^5	8.75×10^{-1}	5.13×10^0	-5.78×10^{-1}
9	4.29×10^8	4.32×10^3	1.35×10^5	8.75×10^{-1}	5.13×10^0	-5.78×10^{-1}
10	2.22×10^8	4.21×10^3	6.19×10^4	8.75×10^{-1}	4.79×10^0	-5.78×10^{-1}
11	2.16×10^8	4.21×10^3	6.19×10^4	8.75×10^{-1}	4.79×10^0	-5.78×10^{-1}
12	9.41×10^7	2.18×10^3	4.25×10^4	8.75×10^{-1}	4.63×10^0	-5.78×10^{-1}
13	8.82×10^7	2.18×10^3	4.25×10^4	8.75×10^{-1}	4.63×10^0	-5.78×10^{-1}
14	3.89×10^7	1.83×10^3	3.10×10^4	8.75×10^{-1}	4.49×10^0	-5.78×10^{-1}
15	3.30×10^7	1.29×10^3	3.10×10^4	8.75×10^{-1}	4.49×10^0	-5.78×10^{-1}
16	2.38×10^7	1.83×10^3	8.38×10^3	8.75×10^{-1}	3.92×10^0	-5.78×10^{-1}
17	1.79×10^7	6.61×10^2	8.38×10^3	8.75×10^{-1}	3.92×10^0	-5.78×10^{-1}
18	1.79×10^7	6.61×10^2	8.38×10^3	8.75×10^{-1}	3.92×10^0	-5.78×10^{-1}

3.3.7 The Raman spectrum of wulfenite

The last Raman spectrum datafile of minerals which we examine is of wulfenite. It consists of 1024 pairs of data which are fed to L2WPMA for each k in $\{1, 2, \dots, 16\}$. The corresponding results are presented in Wulfenite.xlsx. In Fig. 3.17 we display the data and the best fit for $k = 14$ in order to capture the main features of the data sets.

Moreover, for $k = 16$ the method detects 15 turning points, 8 of which are peaks. In order to examine the behavior of the approximation, we display the turning point positions by piecewise monotonic fits to the wulfenite data for values of k in $\{2, 4, \dots, 16\}$ in Table

3.15. In the right part of Table 3.15 we indicate the positions of the turning points of each optimal fit for k in $\{2, 4, \dots, 16\}$ in correspondence with the column labeled “ t_j ”, derived when $k = 16$. For instance, when $k = 4$ the turning points occur at the positions 167, 224 and 704 as indicated by the times signs in the column labeled “4”, while for $k = 6$ two more turning points occur at the positions 600 and 637 as indicated by the times signs in the column labeled “6”.

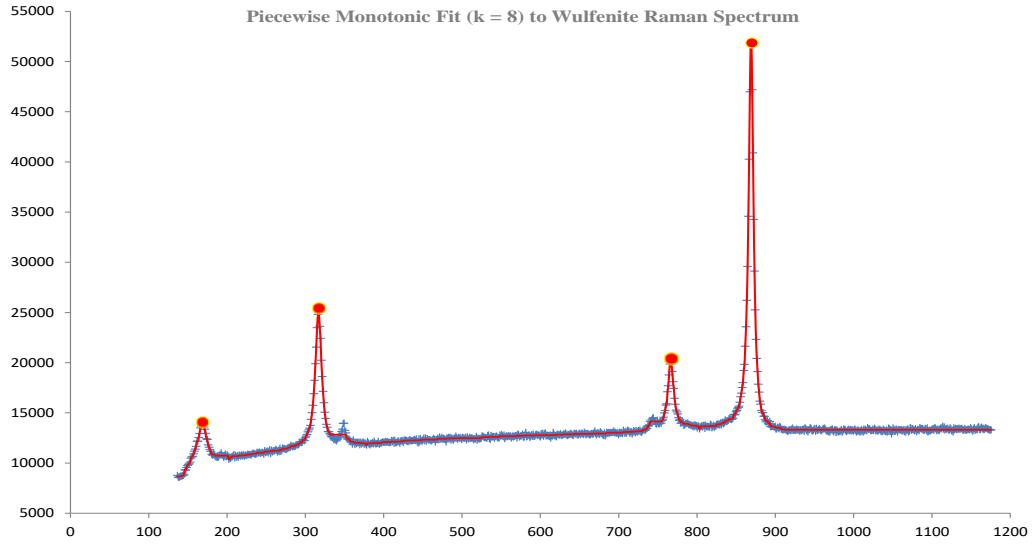


Figure 3.17: Detected peaks (circles) by a best monotonic fit with $k = 8$ to 1024 data points (plus signs) of the wulfenite Raman spectrum. The solid line illustrates the best fit. The numbers give the intensities at the corresponding Raman shifts.

Table 3.15: Left four columns: Turning points in the wulfenite spectrum by a best fit with $k = 16$ monotonic sections. Right eight columns: The turning point positions of the optimal fit for k in $\{2, 4, \dots, 16\}$ are indicated by the times sign

j	t_j	x_{t_j}	Intensity (ϕ_{t_j})	$k =$	2	4	6	8	10	12	14	16
0	1	1.37×10^2	8.78×10^3		×	×	×	×	×	×	×	×
1	30	1.68×10^2	1.38×10^4					×	×	×	×	×
2	61	2.02×10^2	1.04×10^4					×	×	×	×	×
3	167	3.17×10^2	2.50×10^4			×	×	×	×	×	×	×
4	188	3.40×10^2	1.22×10^4						×	×	×	×
5	197	3.49×10^2	1.40×10^4						×	×	×	×
6	224	3.78×10^2	1.18×10^4			×	×	×	×	×	×	×
7	578	7.44×10^2	1.45×10^4								×	×
8	586	7.52×10^2	1.39×10^4								×	×
9	600	7.66×10^2	1.99×10^4				×	×	×	×	×	×
10	637	8.03×10^2	1.34×10^4				×	×	×	×	×	×
11	704	8.69×10^2	5.18×10^4		×	×	×	×	×	×	×	×
12	815	9.78×10^2	1.30×10^4									×
13	857	1.02×10^3	1.35×10^4									×
14	889	1.05×10^3	1.29×10^4							×	×	×
15	958	1.11×10^3	1.37×10^4							×	×	×
16	1024	1.18×10^3	1.33×10^4		×	×	×	×	×	×	×	×

Table 3.16 presents the results of the centralized measures which are mentioned to section 3.1. It is observed that the order of magnitude of the sum of squares starts from 10^{10} for $k = 1$, decreases to 10^9 for $k = 2$ and $k = 3$ and to 10^8 for $k = 4$ and $k = 5$. Then it falls to 10^7 for k in $\{6, 7, 8, 9\}$ and to 10^6 for k in $\{10, 11, \dots, 16\}$. For k in $\{2, 3, \dots, 9\}$ it is equal per two. The maximum absolute value of the estimated errors starts from 3.85×10^4 for $k = 1$ and ends to 3.07×10^2 for k in $\{14, 15, 16\}$. For k in $\{2, 3, \dots, 13\}$ the values are equal per two. The maximum absolute value of nonzero Lagrange multipliers starts from 1.07×10^6 for $k = 1$. For k in $\{2, 3, \dots, 7\}$ it decreases and the values are equal per two. It decreases more to 1.29×10^4 for k in $\{8, 9, 10, 11\}$ and to 2.59×10^3 for k in $\{12, 13, 14, 15\}$. For $k = 16$ it falls to 1.94×10^3 . The minimum absolute value of nonzero Lagrange multipliers is 1.88×10^1 for $k = 1$ and it decreases to 2.00×10^0 for k in $\{2, 3, \dots, 16\}$. Their decadic logarithms have a corresponding behavior.

Table 3.16: Measures for Wulfenite

k	SSR	D	L	ℓ	$\log_{10}L$	$\log_{10}\ell$
1	1.14×10^{10}	3.85×10^4	1.07×10^6	1.88×10^1	6.03×10^0	1.27×10^0
2	1.28×10^9	1.22×10^4	2.32×10^5	2.00×10^0	5.36×10^0	3.01×10^{-1}
3	1.28×10^9	1.22×10^4	2.32×10^5	2.00×10^0	5.36×10^0	3.01×10^{-1}
4	2.83×10^8	5.38×10^3	9.18×10^4	2.00×10^0	4.96×10^0	3.01×10^{-1}
5	2.83×10^8	5.38×10^3	9.18×10^4	2.00×10^0	4.96×10^0	3.01×10^{-1}
6	7.46×10^7	2.64×10^3	5.12×10^4	2.00×10^0	4.71×10^0	3.01×10^{-1}
7	7.46×10^7	2.64×10^3	5.12×10^4	2.00×10^0	4.71×10^0	3.01×10^{-1}
8	1.39×10^7	1.16×10^3	1.29×10^4	2.00×10^0	4.11×10^0	3.01×10^{-1}
9	1.39×10^7	1.16×10^3	1.29×10^4	2.00×10^0	4.11×10^0	3.01×10^{-1}
10	9.17×10^6	4.19×10^2	1.29×10^4	2.00×10^0	4.11×10^0	3.01×10^{-1}
11	9.14×10^6	4.19×10^2	1.29×10^4	2.00×10^0	4.11×10^0	3.01×10^{-1}
12	8.07×10^6	3.70×10^2	2.59×10^3	2.00×10^0	3.41×10^0	3.01×10^{-1}
13	8.04×10^6	3.70×10^2	2.59×10^3	2.00×10^0	3.41×10^0	3.01×10^{-1}
14	7.62×10^6	3.07×10^2	2.59×10^3	2.00×10^0	3.41×10^0	3.01×10^{-1}
15	7.59×10^6	3.07×10^2	2.59×10^3	2.00×10^0	3.41×10^0	3.01×10^{-1}
16	7.37×10^6	3.07×10^2	1.94×10^3	2.00×10^0	3.29×10^0	3.01×10^{-1}

3.4 Experiments on turning point separation

In this section we present two more experiments, one of MS spectrum datafile and one of Raman spectrum datafile, which show a different behavior than the corresponding datafiles of sections 3.2 and 3.3. We have seen in these sections that as k increases by 2, the turning points are maintained. Nonetheless, we notice here, that is behavior no longer holds.

3.4.1 The MS spectrum of diiodothyronine

In the next experiment we use a MS spectrum datafile of thyroid hormone diiodothyronine. The number of pairs of data is 2167. Feeding the data to L2WPMA for k in $\{1, 2, \dots, 16\}$, we obtain the results which are presented in Diiodothyronine.xlsx, one sheet for each k , with the calculations of the measures which we study. Fig. 3.18 shows the main features of the data sets, that is the data and the best fit for $k = 16$.

In addition, for $k = 16$ the method detects 15 turning points, 8 of which are peaks. Table 3.17 presents the turning point positions by piecewise monotonic fits to the diiodothyronine data for values of k in $\{2, 4, \dots, 16\}$, so that we explore the behavior of the approximation. In the right part of Table 3.17 we indicate the positions of the turning points of each optimal fit for k in $\{2, 4, \dots, 16\}$ in correspondence with the column labeled “ t_j ”, derived when $k = 16$. For instance, when $k = 6$ the turning points occur at the positions 1569, 1743, 1910, 2000 and 2107 as indicated by the times signs in the column labeled “6”. When $k = 8$ two more turning points occur at the positions 2050 and 2087 as indicated by the times signs in the column labeled “8”. The turning point at the position 2000 when $k = 6$ is shifting into the position 1990 when $k = 8$.

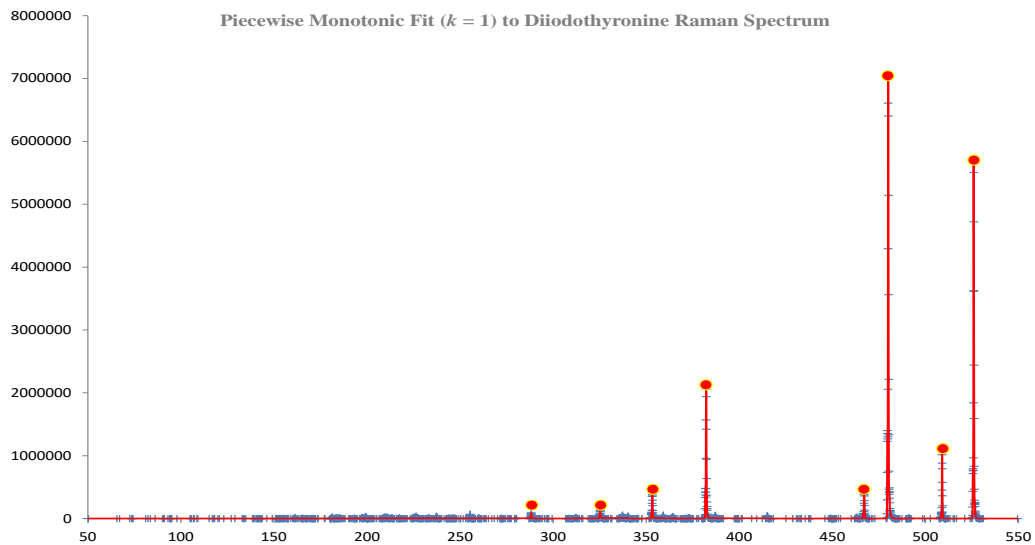


Figure 3.18: Detected peaks (circles) by a best monotonic fit with $k = 16$ to 2167 data points (plus signs) of the diiodothyronine Raman spectrum. The solid line illustrates the best fit. The numbers give the intensities at the corresponding Raman shifts.

So far we have been seen that as k increases to $k + 2$ the positions of the turning points are maintained. It is quite interesting that the fit to this data set shows a shifting of some turning points as k increases by 2. For instance, we see in Table 3.17 that the fourth turning point when $k = 10$ has moved from position 1889 to position 1891 when $k = 12$. Similarly,

the fourth turning point when $k = 6$ has moved from position 2000 to position 1990 when $k = 8$. This phenomenon is explained by the property that the optimal turning point for given k is separated by the optimal turning point when $k + 1$ (see [15]).

Table 3.17: Left four columns: Turning points in the diiodothyronine spectrum by a best fit with $k = 16$ monotonic sections. Right eight columns: The turning point positions of the optimal fit for k in $\{2, 4, \dots, 16\}$ are indicated by the times sign^a

j	t_j	x_{t_j}	Intensity (ϕ_{t_j})	$k =$	2	4	6	8	10	12	14	16
0	1	5.03×10^1	4.58×10^2		×	×	×	×	×	×	×	×
1	899	2.88×10^2	9.13×10^4									×
2	938	2.92×10^2	1.96×10^2									×
3	1076	3.25×10^2	1.37×10^5								×	×
4	1253	3.43×10^2	1.96×10^2								×	×
5	1297	3.53×10^2	3.80×10^5							×	×	×
6	1453	3.66×10^2	1.96×10^2							×	×	×
7	1569	3.82×10^2	2.10×10^6				×	×	×	×	×	×
8	1743	4.17×10^2	1.96×10^2				×	×	×	×	×	×
9	1848	4.67×10^2	4.35×10^5						×	×	×	×
10	1891	4.70×10^2	2.48×10^2						□	×	×	×
11	1910	4.80×10^2	7.03×10^6		×	×	×	×	×	×	×	×
12	1990	4.85×10^2	2.41×10^2			○	○	×	×	×	×	×
13	2050	5.09×10^2	1.02×10^6					×	×	×	×	×
14	2089	5.16×10^2	1.96×10^2					◇	◇	×	×	×
15	2107	5.26×10^2	5.73×10^6			×	×	×	×	×	×	×
16	2167	5.49×10^2	2.75×10^2		×	×	×	×	×	×	×	×

^a × = the number in column labeled “ t_j ”, □ = 1889, ○ = 2000, ◇ = 2087

Table 3.18 presents the values of the centralized measures for each k in $\{1, 2, \dots, 16\}$ of the above results and their calculations. It is observed that the sum of squares of residuals decreases while the number of monotonic sections increases. More specifically, its order of magnitude is 10^{14} for k in $\{1, 2, 3\}$. It decreases to 2.37×10^{13} for $k = 4$ and $k = 5$ and to 4.26×10^{12} for $k = 6$ and $k = 7$. Then it falls to 1.53×10^{12} for $k = 8$ and $k = 9$, to 8.37×10^{11} for $k = 10$ and $k = 11$ and to 2.10×10^{11} for $k = 12$ and $k = 13$. For $k = 14$ and $k = 15$ it decreases more to 1.38×10^{11} and for $k = 16$ to 1.07×10^{11} . The maximum absolute value of estimated errors falls as k increases. Its order of magnitude is 10^6 for k in $\{1, 2, \dots, 5\}$. Then it falls to 10^5 for k in $\{6, 7, \dots, 13\}$ and 10^4 for k in $\{14, 15, 16\}$. The values for k in $\{4, 5, \dots, 16\}$ are equal per two. A reduction in the order of magnitude also occurs in the maximum absolute value of nonzero Lagrange multiplies. More specifically, it starts from 10^7 for k in $\{1, 2, \dots, 5\}$, it decreases to 10^6 for k in $\{7, 8, \dots, 15\}$ and to 10^5 for $k = 16$. The minimum absolute value of the nonzero Lagrange multipliers presents a fluctuation for k in $\{1, 2, \dots, 11\}$, that is for $k = 1$ and $k = 3$ the value is equal

to 1.78×10^1 , for $k = 5$ and $k = 7$ is equal to 1.07×10^1 and for $k = 9$ and $k = 11$ is equal to 4.56×10^0 . For k in $\{2, 4, 6, 8, 10\}$ the value is equal to 5.70×10^0 . The value falls for k in $\{12, 13, \dots, 16\}$ to 4.02×10^0 . Their decadic logarithms have a corresponding behavior.

Table 3.18: Measures for Diiodothyronine

k	SSR	D	L	ℓ	$\log_{10}L$	$\log_{10}\ell$
1	3.30×10^{14}	6.74×10^6	8.58×10^7	1.78×10^1	7.93×10^0	1.25×10^0
2	1.43×10^{14}	5.50×10^6	6.28×10^7	5.70×10^0	7.80×10^0	7.56×10^{-1}
3	1.32×10^{14}	5.20×10^6	5.30×10^7	1.78×10^1	7.72×10^0	1.25×10^0
4	2.37×10^{13}	2.04×10^6	2.84×10^7	5.70×10^0	7.45×10^0	7.56×10^{-1}
5	2.37×10^{13}	2.04×10^6	2.84×10^7	1.07×10^1	7.45×10^0	1.03×10^0
6	4.26×10^{12}	9.19×10^5	7.38×10^6	5.70×10^0	6.87×10^0	7.56×10^{-1}
7	4.26×10^{12}	9.19×10^5	7.38×10^6	1.07×10^1	6.87×10^0	1.03×10^0
8	1.53×10^{12}	3.80×10^5	5.19×10^6	5.70×10^0	6.72×10^0	7.56×10^{-1}
9	1.53×10^{12}	3.80×10^5	5.19×10^6	4.56×10^0	6.72×10^0	6.59×10^{-1}
10	8.37×10^{11}	3.65×10^5	5.19×10^6	5.70×10^0	6.72×10^0	7.56×10^{-1}
11	8.37×10^{11}	3.65×10^5	5.19×10^6	4.56×10^0	6.72×10^0	6.59×10^{-1}
12	2.10×10^{11}	1.26×10^5	1.70×10^6	4.02×10^0	6.23×10^0	6.04×10^{-1}
13	2.10×10^{11}	1.26×10^5	1.70×10^6	4.02×10^0	6.23×10^0	6.04×10^{-1}
14	1.38×10^{11}	8.53×10^4	1.13×10^6	4.02×10^0	6.05×10^0	6.04×10^{-1}
15	1.38×10^{11}	8.53×10^4	1.13×10^6	4.02×10^0	6.05×10^0	6.04×10^{-1}
16	1.07×10^{11}	6.94×10^4	7.09×10^5	4.02×10^0	5.85×10^0	6.04×10^{-1}

3.4.2 The Raman spectrum of cellulose

The last Raman spectrum datafile is of carbohydrate cellulose. It consists of 3590 pairs of data sets and is tested for k in $\{1, 2, \dots, 18\}$. We feed the data to L2WPMA for each value of k . The corresponding results are presented in Cellulose.xlsx, one sheet for each k . The main features of the data sets for $k = 16$ may be captured by looking at Fig. 3.19.

Furthermore, for $k = 18$ the method detects 17 turning points, 9 of which are peaks. The behavior of the approximation is explored by presenting in Table 3.19 the turning point positions by piecewise monotonic fits to the cellulose data for values of k in $\{2, 4, \dots, 18\}$. In the right part of Table 3.19 we display the positions of the turning points of each optimal fit for k in $\{2, 4, \dots, 18\}$ in correspondence with the column labeled ‘ t_j ’, derived when $k = 18$. For example, when $k = 6$ the turning points occur at the positions 368, 795, 1084, 2421 and 2884 as indicated by the times signs in the column labeled ‘‘6’’ and when $k = 8$ the method detects two more turning points at the positions 1204 and 1368 as indicated by the times signs in the column labeled ‘‘8’’.

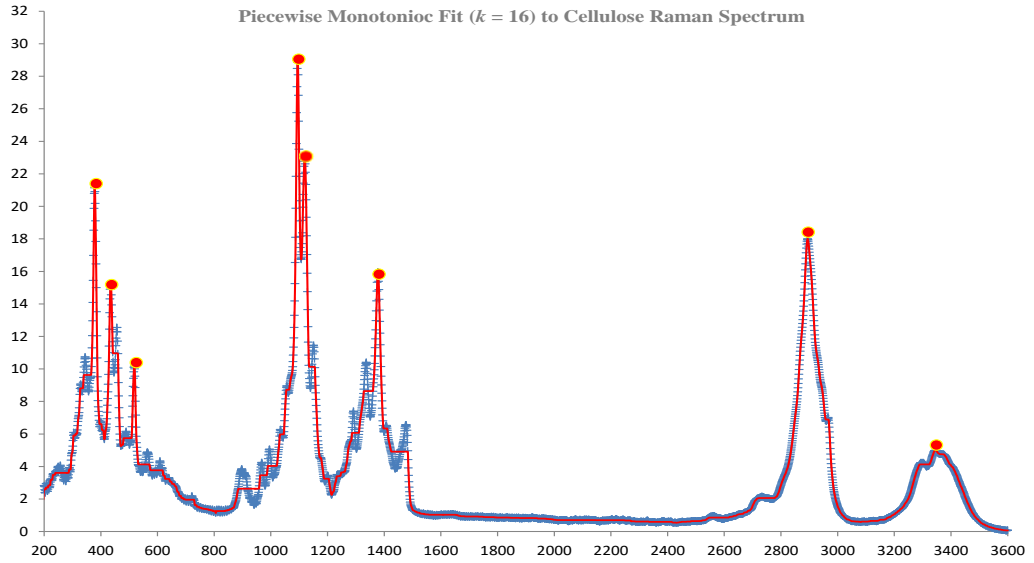


Figure 3.19: Detected peaks (circles) by a best monotonic fit with $k = 16$ to 3590 data points (plus signs) of the cellulose Raman spectrum. The solid line illustrates the best fit. The numbers give the intensities at the corresponding Raman shifts.

Table 3.19: Left four columns: Turning points in the cellulose spectrum by a best fit with $k = 18$ monotonic sections. Right nine columns: The turning point positions of the optimal fit for k in $\{2, 4, \dots, 18\}$ are indicated by the times sign

j	t_j	x_{t_j}	Intensity (ϕ_{t_j})	$k =$	2	4	6	8	10	12	14	16	18
0	1	1.10×10^1	7.46×10^{-1}		×	×	×	×	×	×	×	×	×
1	368	3.78×10^2	2.11×10^1				×	×	×	×	×	×	×
2	402	4.12×10^2	5.67×10^0							×	×	×	×
3	425	4.35×10^2	1.52×10^1							×	×	×	×
4	461	4.71×10^2	5.25×10^0								×	×	×
5	508	5.18×10^2	1.02×10^1								×	×	×
6	795	8.05×10^2	1.14×10^0				×	×	×	×	×	×	×
7	1084	1.09×10^3	2.90×10^1		×	×	×	×	×	×	×	×	×
8	1097	1.11×10^3	1.67×10^1									×	×
9	1109	1.12×10^3	2.29×10^1									×	×
10	1204	1.21×10^3	2.25×10^0					×	×	×	×	×	×
11	1326	1.34×10^3	1.04×10^1										×
12	1341	1.35×10^3	7.06×10^0										×
13	1368	1.38×10^3	1.60×10^1					×	×	×	×	×	×
14	2421	2.43×10^3	5.40×10^{-1}			×	×	×	×	×	×	×	×
15	2884	2.89×10^3	1.80×10^1			×	×	×	×	×	×	×	×
16	3072	3.08×10^3	5.85×10^{-1}						×	×	×	×	×
17	3335	3.35×10^3	4.99×10^0						×	×	×	×	×
18	3590	3.60×10^3	8.14×10^{-2}		×	×	×	×	×	×	×	×	×

The values of measures which are examined are presented in Table 3.20. While the number of monotonic sections k increases, the order of magnitude of the sum of squares of errors decreases. More specifically, it starts from 10^4 for k in $\{1, 2, \dots, 5\}$, decreases to 10^3 for k in $\{6, 7, \dots, 11\}$ and to 10^2 for k in $\{12, 13, \dots, 18\}$. Respectively, a decrease is observed in the maximum absolute values of estimated errors. For $k = 1$ its value is

equal to 2.39×10^1 , decreases to 1.66×10^1 for k in $\{2, 3, 4, 5\}$ and to 9.79×10^0 for $k = 6$ and $k = 7$. Then it falls to 6.02×10^0 for k in $\{8, 9, 10, 11\}$. For k in $\{12, 13, \dots, 17\}$ the value is equal per two and for $k = 18$ it falls to 1.66×10^0 . The maximum value of non zero Lagrange multipliers is 2.83×10^3 for k in $\{1, 2, 3\}$, it decreases to 1.90×10^3 for $k = 4$ and $k = 5$, to 6.68×10^2 for k in $\{6, 7, 8, 9\}$ and to 1.87×10^2 for $k = 10$ and $k = 11$. For k in $\{12, 13, \dots, 18\}$ a fluctuation is observed, that is for k in $\{12, 14, 16, 18\}$ the value is equal to 4.75×10^1 , for $k = 13$ is equal to 6.42×10^1 and for $k = 15$ and $k = 17$ is equal to 5.13×10^1 . The minimum absolute value of nonzero Lagrange multipliers is 3.58×10^{-4} for $k = 1$ and $k = 2$. It falls to 2.15×10^{-4} for $k = 3$ and to 4.70×10^{-5} for k in $\{4, 5, \dots, 18\}$. The behavior of their decadic logarithms follows the same pattern.

Table 3.20: Measures for Cellulose

k	SSR	D	L	ℓ	$\log_{10}L$	$\log_{10}\ell$
1	4.49×10^4	2.39×10^1	2.83×10^3	3.58×10^{-4}	3.45×10^0	-3.45×10^0
2	2.73×10^4	1.66×10^1	2.83×10^3	3.58×10^{-4}	3.45×10^0	-3.45×10^0
3	2.72×10^4	1.66×10^1	2.83×10^3	2.15×10^{-4}	3.45×10^0	-3.67×10^0
4	1.28×10^4	1.66×10^1	1.90×10^3	4.70×10^{-5}	3.28×10^0	-4.33×10^0
5	1.28×10^4	1.66×10^1	1.90×10^3	4.70×10^{-5}	3.28×10^0	-4.33×10^0
6	4.65×10^3	9.79×10^0	6.68×10^2	4.70×10^{-5}	2.82×10^0	-4.33×10^0
7	4.62×10^3	9.79×10^0	6.68×10^2	4.70×10^{-5}	2.82×10^0	-4.33×10^0
8	2.26×10^3	6.02×10^0	6.68×10^2	4.70×10^{-5}	2.82×10^0	-4.33×10^0
9	2.22×10^3	6.02×10^0	6.68×10^2	4.70×10^{-5}	2.82×10^0	-4.33×10^0
10	1.10×10^3	6.02×10^0	1.87×10^2	4.70×10^{-5}	2.27×10^0	-4.33×10^0
11	1.07×10^3	6.02×10^0	1.87×10^2	4.70×10^{-5}	2.27×10^0	-4.33×10^0
12	5.06×10^2	3.78×10^0	7.45×10^1	4.70×10^{-5}	1.87×10^0	-4.33×10^0
13	4.71×10^2	3.78×10^0	6.42×10^1	4.70×10^{-5}	1.81×10^0	-4.33×10^0
14	3.87×10^2	3.10×10^0	7.45×10^1	4.70×10^{-5}	1.87×10^0	-4.33×10^0
15	3.52×10^2	3.10×10^0	5.13×10^1	4.70×10^{-5}	1.71×10^0	-4.33×10^0
16	2.70×10^2	1.77×10^0	7.45×10^1	4.70×10^{-5}	1.87×10^0	-4.33×10^0
17	2.35×10^2	1.77×10^0	5.13×10^1	4.70×10^{-5}	1.71×10^0	-4.33×10^0
18	2.26×10^2	1.66×10^0	7.45×10^1	4.70×10^{-5}	1.87×10^0	-4.33×10^0

Chapter 4

Discussion and Conclusions

In this chapter we state the conclusions about the experiments, which are mentioned in chapter 3, that may lead to the determination of the relationship between the number of monotonic sections and Lagrange multipliers in a piecewise monotonic approximation.

In chapter 1 we discussed the problem of data approximation and especially the case of least squares data fitting in which the sum of squares of residuals are minimized. We presented how the smoothed data are calculated and we made a first reference to the piecewise monotonic approximation method. Moreover, we discussed the non-linear programming problem and Lagrange multipliers in both cases when the constraints are linear equality and linear inequality. More specifically, we stated the case that the objective function is a quadratic function and the theorem of Karush-Kuhn-Tucker.

In chapter 2 we presented the piecewise monotonic data approximation as a data smoothing approach which can have many applications. We started with a definition of the method and its main features. Then we discussed the monotonic problem, which is a strictly quadratic problem, and we stated an example that gives the best approximation to data from a function which we created. Last, we stated how the Lagrange multipliers are calculated in the monotonic case.

In chapter 3 we performed experiments using ten Raman spectrum datafiles, eight of minerals, one of carbohydrate and one of thyroid hormone, in order to determine how Lagrange multipliers are changed as the number of monotonic sections in a piecewise monotonic data approximation is changed. We defined the measures which are needed to determine this relationship and then we fitted each data by the L2WPMA software package for various values of monotonic sections. These applications showed the effectiveness of piecewise monotonic approximation to peak estimation of spectra that are represented by

some noisy measurements of their values. Although the optimization calculation may have a very large number of local minima, we have procedures that obtain a global solution in quadratic complexity with respect to n .

Subsequently, in chapter 3 figures and tables were presented with the results of the calculations in order to capture the main features of each data set. Furthermore, the measures which were mentioned in section 3.1 were calculated and presented in centralized tables in order to compare the behavior of these measures as the number of monotonic sections is changed.

From the research we concluded that the sum of squares of residuals decreases while the number of monotonic sections increases, in all cases. Its order of magnitude decreases while the method detects fewer and fewer not so important peaks. The maximum absolute value of estimated errors also decreases while the number of monotonic sections increases. Moreover, the order of magnitude of maximum absolute value of nonzero Lagrange multipliers while the number of monotonic sections increases and the method detects not so important peaks. There are cases where the minimum absolute value of nonzero Lagrange multipliers decreases gradually while the number of monotonic sections increases, as we saw in Table 3.4, Table 3.6, Table 3.8, Table 3.14, Table 3.16, Table 3.18, cases where there was a fluctuation in its value while the number of monotonic sections increases, as we saw in Table 3.2 and Table 3.20, and cases where it remained stable while the monotonic sections increases, as we saw in Table 3.10 and Table 3.12. The behavior of their decadic logarithms follows the same pattern.

As it comes from the theory of general non-linear programming, the size of the Lagrange multipliers provides an indication of the importance of the corresponding constraints, and it also shows the magnitude of change of the objective function as k increases. This will be highly valuable to the development of a Lagrange multiplier test that will provide an estimate of a suitable or adequate number of monotonic sections of the fit.

Bibliography

- [1] C. F. Gauss, *Theory of the Combination of Observations Least Subject to Errors, Part One, Part Two, Supplement*, Classics in Applied Mathematics, Society for Industrial and Applied Mathematics, Facsimile edition, 1987
- [2] C. de Boor, *A Practical Guide to Splines, Revised Edition*, NY: Springer-Verlag, Applied Mathematical Sciences, vol. 27, 2001.
- [3] A. P. Bruner, K. Scott, D. Wilson, B. Underhill, T. Lyles, C. Stopka, R. Ballinger and E. A. Geiser, “*Automatic Peak Finding of Dynamic Batch Sets of Low SNR In-Vivo Phosphorus NMR Spectra*”, unpublished manuscript, Departments of Radiology, Physics, Nuclear and Radiological Sciences, Surgery, Mathematics, Medicine, and Exercise and Sport Sciences, University of Florida, and the Veterans Affairs Medical Center, Gainesville, Florida, U.S.
- [4] P. Dierckx, *Curve and surface Fitting with Splines*, Oxford: Clarendon Press, 1995.
- [5] W. Cheney and W. Light, *A Course in Approximation Theory*, NY: Brooks/Cole Publishing Company, An International Thompson Publishing Company, 2000.
- [6] F. B. Hildebrand, *Introduction to Numerical Analysis*, Second Edition, Dover Publications, Inc., New York, 1987.
- [7] G. E. Forsythe, M. A. Malcolm, C. B. Moler, *Computer methods for mathematical computations*, Prentice-Hall, Inc., Englewood Cliffs, New Jersey, 1977.
- [8] J. C. G. Boot, *Quadratic Programming*, North Holland, Amsterdam, 1964.
- [9] R. Fletcher, *Practical Methods of Optimization*, Second Edition, Wiley, Chichester, 1974.
- [10] G. R. Walsh, *Methods of Optimization*, Wiley, Chichester, 1974.

- [11] M. J. D. Powell, *Gradient conditions and Lagrange multipliers in nonlinear programming in "Nonlinear Optimization Theory and Algorithms"* (L. C. W. Dixon, ed.), pp. 201 - 220, 1980.
- [12] I. C. Demetriou, *Data smoothing by Piecewise Monotonic Divided Differences*, Ph.D. Dissertation, Department of Applied Mathematics and Theoretical Physics, University of Cambridge, Cambridge, 1985.
- [13] I. C. Demetriou, "*Discrete piecewise monotonic approximation by a strictly convex distance function*", *Mathematics of Computation*, vol. 64, 209, pp. 157 - 180, 1995.
- [14] I. C. Demetriou, "*Algorithm 863: L2WRMA, a fortran 77 package for weighted least-squares piecewise monotonic data approximation*", *ACM Trans. Math. Softw.*, vol. 33, 1, pp. 1 - 19, 2007.
- [15] I. C. Demetriou, *Separation theorems for the extrema of best piecewise monotonic approximations to successive data*, unpublished manuscript, 20 pp., 2019.
- [16] I. C. Demetriou and M. J. D. Powell, "*Least squares smoothing of univariate data to achieve piecewise monotonicity*", *IMA J. of Numerical Analysis*, vol. 11, pp. 411 - 432, 1991.
- [17] C. van Eeden, *Maximum Likelihood Estimation of Ordered Probabilities*, *Indagationes Mathematicae*, 18 (1956), 444-455.
- [18] J. Lu, "*Signal restoration with controlled piecewise monotonicity constraint*", *Proceedings of the IEEE International Conference on Acoustics, Speech and Signal Processing*, 12 May 1998 - 15 May 1998, Scattle WA, vol. 3, pp. 1621 - 1624, 1998.
- [19] Y. X. Yuan, *A review of subspace methods for nonlinear optimization*, *Proceedings of the International Congress of Mathematics*, pp. 807 - 827, 2014.
- [20] Y. X. Yuan, *A review of trust region algorithms for optimization*, *Iciam*, vol. 99, pp. 271 - 282, 2000.
- [21] W. Y. Sun and Y. X. Yuan, *Optimization Theory and Methods: Nonlinear Programming*, Springer Verlag, New York, 2006.
- [22] M. J. D. Powell, "*Curve fitting by splines in one variable*", in *Numerical Approximation to Functions and Data*, ed. J. G. Hayes, The Institute of Mathematics and its Applications, London, U.K.: The Athlone Press, pp. 65 - 83, 1970.

- [23] E. Vassiliou and I. C. Demetriou, “An adaptive algorithm for least squares piecewise monotonic data fitting”, *Computational Statistics and Data Analysis*, vol. 49, pp. 591 - 609, 2005.
- [24] C. Lanczos, *Evaluation of noisy data*, SIAM Journal on numerical analysis, Ser. B, vol. 1, U.S.A., 1964.
- [25] Department of Physics, University of Parma. Available online: <http://www.fis.unipr.it/phevix/ramandb.php>, Database, Laboratory of Photoinduced Effects Vibrational and X-RAYS Spectroscopies, Minerals, Zircon1.txt, Clintonite1.txt, Olivenite1.txt, Datolite1.txt, Beryl2.txt, Lizardite.txt, Hemimorphite.txt, Wulfenite.txt, accessed on 12 December 2018.
- [26] Canadian Institutes of Health Research, Canada Foundation for Innovation and The Metabolomics Innovation Centre (TMIC). Available online: <http://www.hmdb.ca/metabolites>, Database, Human Metabolome Database, Diiodothyronine.txt, accessed 10 January 2019
- [27] Department of Food Science, Faculty of Science, University of Copenhagen. Available online: <http://www.models.life.ku.dk/specarb/specarb.html>, Database, SPECARB, Polysaccharides, Polymonosaccharides, Cellulose.txt, accessed on 10 December 2018.